HPD COURIER

NUMBER 7 | August 2024

20 years of R&D activities for developing a new generation of RPC & TRD

Electronic version
HPD Couriers can be accessed at:
http://niham.nipne.ro/HPD_Courier.html

Motivation

The experimental study of different regions of the complex phase diagram of strongly interacting matter, including critical points and phase boundaries predicted by QCD requires heavy ion collisions below SPS energies and high-intensity beams, allowing for multi-differential analysis and the measurement of rare probes. Exploration of the QCD phase diagram at large baryon chemical potential began at AGS in Brookhaven and SPS in CERN (at low energies). These experiments, constrained by the detector technologies of that time, were limited to a narrow range of abundantly produced hadrons.
The STAR collaboration at RHIC, through the beam energy scan program, conducted measurements from $\sqrt{s_{NN}} = 200$ GeV down to 7.7 GeV in Au+Au collisions, and even lower (3 GeV) in fixed-target experiments. However, due to TPC-readout time and RHIC accelerator luminosity limitations, the reaction rates ranged from about 800 Hz to a few Hz at the lowest energies. Consequently, detailed multi-differential analysis is not feasible at existing facilities.
This limitation motivated the innitiative of the Facility for Antiproton and Ion Research (FAIR) at Darmstadt. SIS100 at FAIR is expected to deliver unprecedented interaction rates (10^7 Hz) at a center of mass energy up to $\sqrt{s_{NN}} = 4.9$ GeV for gold beams.

The Compressed Baryonic Matter (CBM) experiment at FAIR is a fixed target experiment designed to run at interaction rates up to 10 MHz for selected observables, 1-5 MHz for multi-strange hyperons and dileptons, and 100 kHz for open charm measurements without any online event selection. The CBM detector will have a polar acceptance between 2.5 to 25 degrees to cover the small polar angular range at midrapidity. By combining SIS100's high-intensity beams with the high rate/high multiplicity performance of the CBM experimental setup, unique conditions for a comprehensive series of experiments aimed at producing and understanding QCD matter at high net-baryon densities will be provided.
To meet these requirements, a new generation of detectors, front-end electronics, acquisition architectures and data processing were necessary, achieving performance levels of current experiments but for significantly higher counting rates. Our group has developed (over the years) state-of-the-art two-dimensional position-sensitive Multi Strip Multi Gap Resistive Plate Counters (MSMGRPC) and two-dimensional position-sensitive Transition Radiation Detectors (TRD) with dedicated front-end electronics and data processing for the most demanding regions (small polar angles) of the CBM-ToF and TRD subdetectors. The following is an overview of the main activities and results obtained over the last 20 years in these R&D segments.

MSMGRPCs

Triggered by the FOPI Collaboration's need to replace the Plastic Barrel surrounding the Central Drift Chamber (CDC) and after evaluating the performance and drawbacks of timing resistive plate chambers, we proposed a novel concept: the symmetric multi-gap glass resistive plate chamber with multi-strip anodes (MSMGRPC) [M. Petrovici et al., NIPNE Scientific Report 1999, p.59; M. Petrovici et al, VI Workshop on RPC and Related Detectors, Coimbra, Portugal, 26-27, November, 2001; M. Petrovici et al. NIM, A487(2002)337; M. Petrovici et al. NIM, A508(2003)75].

Figure 1

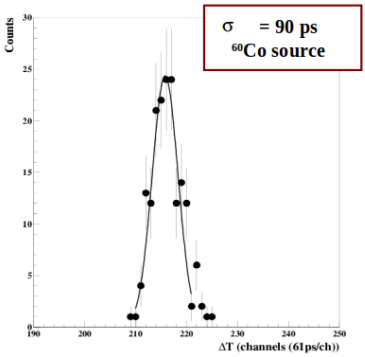

Figure 2

Fig.1 shows the components of the first prototype, and Fig.2 presents a time spectrum obtained using a ^{60}Co radioactive source.

After several years of R&D, the new ToF Barrel of the FOPI experiment, based on this architecture and using float glass as resistive electrodes, significantly improved the particle identification performance [M. Kis et al., NIM A646(2011)27].

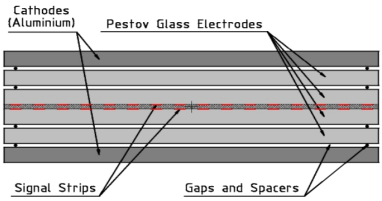

Figure 3

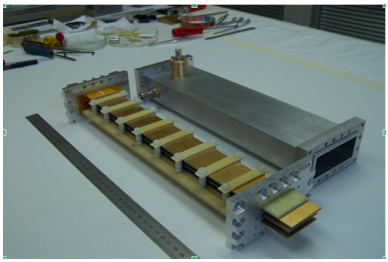

Figure 4

The first high-counting-rate MSMGRPC prototype used a special low-resistivity glass as resistive plate electrodes [A. R. Forlov et al., NIM, A307 (1991) 497]. Figures 3 and 4 show the counter structure and assembled prototype, respectively. The counter was operated at 3.1 kV per gap with a standard gas mixture (85% $C_2F_4H_2$, 10% SF_6, and 5% C_4H_10). Signals were amplified by fast broadband amplifiers developed for the FOPI ToF Barrel [M. Ciobanu et al., IEEE 54(4) (2007) 1201]. Fig.5 shows the experimental configuration for in-house tests using

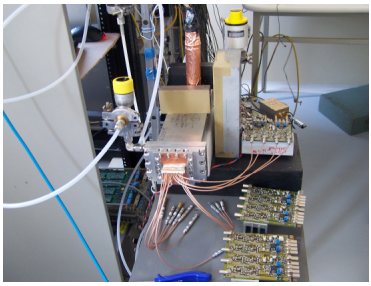

Figure 5

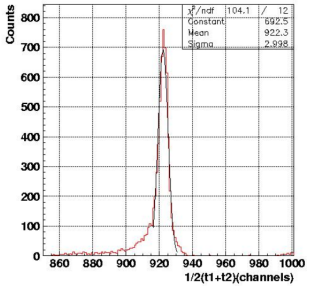

Figure 6

a ^{60}Co source. An example of the time spectrum is shown in Fig.6, demonstrating a time resolution of 50 ps for the MSMGRPC prototype, after accounting for the plastic scintillator's time resolution.
For in-beam tests, we developed two additional MSMGRPC prototypes with differential signal readout: one with strip architecture and one with pad architecture. Fig.7 shows the structures of these prototypes, and Fig.8 shows the assembled prototypes.

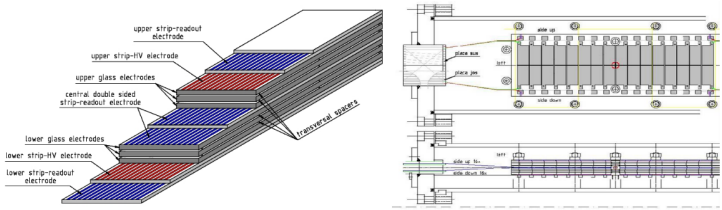

Figure 7

These prototypes had similar configurations as the first one, with the difference that on each side, behind the cathode HV strip structure electrode, separated by a 0.1 mm mylar foil a PCB with copper pickup signal strips was added. Signals from corresponding strips of the cathode signal PCBs were summed up and fed into the input of a differential amplifier together with the anode signal of the corresponding strip. An 8-channel amplifier/discriminator based on the NINO ASIC chip, developed within the ALICE Collaboration [F. Anghinolfi et al., NIM

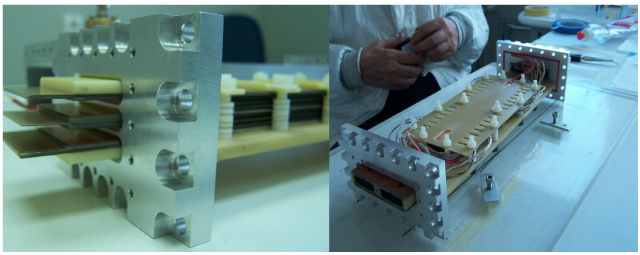

Figure 8

A533(2004)183], provided the ToF information and time over threshold (ToT) for slewing correction.
They were tested at the ELBE electron linac at Forschungzentrum Dresden-Rossendorf. A 30 MeV electron beam with ∼5 ps pulse resolution scattered at 45° by an 18 μm Al foil illuminated the full surface of the tested RPCs. Fig.9 shows a sketch (left) of the experimental configuration and a photo (right), respectively.

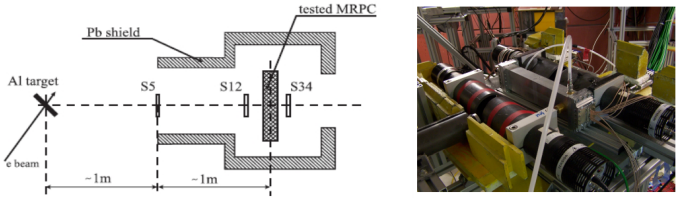

Figure 9

Time resolution without and with slewing correction for the first MSMGRPC prototype is shown in Fig.10 (left), while similar plots for the differential readout MSMGRPC prototype are shown in Fig.10 (right). Time resolutions of ∼50 ps and 70 ps were achieved, with no degradation up to 16 kHz/cm².

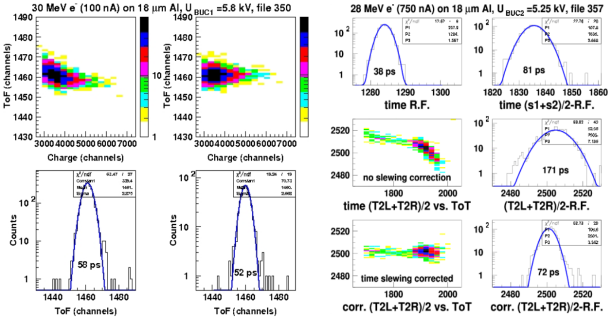

Figure 10

The time resolution as a function of counting rate for the second prototype is presented in Fig.11 [D. Bartos et al., 2008 NSS/MIC,Vols.1-9 Book Series:IEEE Nuclear Science Symposium - Conf. Rec. pg: 1933; M. Petris et al., Rom. Jour. Phys. 56(2011)349].

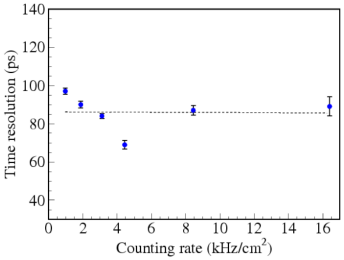

Figure 11

A new differential configuration based on a high granularity strip structure was designed and built to meet granularity requirements for high multiplicity environments (Fig.12).

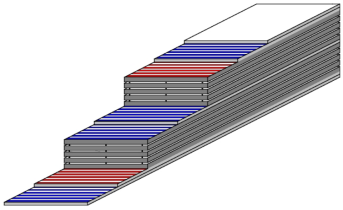

Figure 12

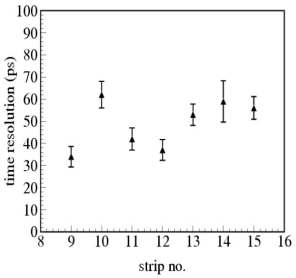

Figure 13

The counter had a symmetrical structure of 2×5 gaps of 140 μm each, with resistive electrodes made from 0.5 mm thick commercial float glass ($\sim 10^{12}\Omega$cm resistivity). The readout electrodes had a strip structure (2.5 mm pitch, 1.1 mm width) with a strip length of 46 mm. High voltage electrodes had the same strip structure. The MSMGRPC with an active area was 46×180 mm^2, read out with 72 strips was housed in a gas-tight rectangular aluminum box.

Initial tests with a ^{60}Co source used a high voltage of 1.98 kV/gap and a gas mixture (85% $C_2F_4H_2$, 10% SF_6, 5% C_4H_{10}) at normal pressure, with differential readout electronics based on NINO chips.

In-beam tests were performed at SIS18 accelerator from GSI-Darmstadt, within a joint measurement campaign of the CBM-TOF Collaboration, using secondary particles produced by a 3.1 GeV/c proton beam on a Pb target. The single counter

time resolution for the measured strips is shown in Fig.13. An average time resolution of ∼50 ps was achieved [D. Bartos et al., CBM Progress Report 2009, pg. 39; M. Petris et al., NIMA661(2012)S129].

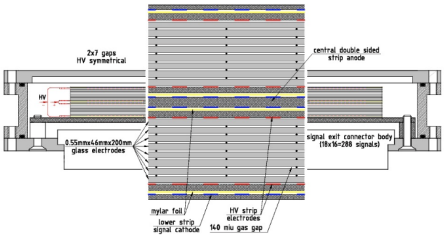

Figure 14

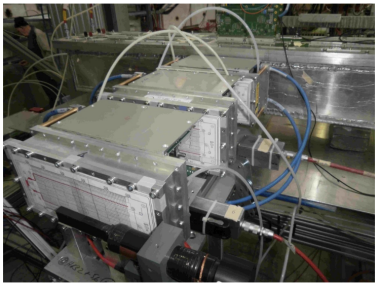

Figure 15

Based on these promising results, new prototypes with a completely two stacks symmetric architecture relative to the median plane were developed (Fig.14). This structure allows for lower applied voltage values on both cathode and anode electrodes. The strip configuration remained the same as of theprevious prototypes: 2.54 mm pitch, 1.1 mm strip width, 1.44 mm spacing between strips, and 46 mm strip length. Three such prototypes were built. Each prototype had 72 strips defining an active area of 46×180 mm^2. The differences were as follows: RPC1 had strip-structured high voltage electrodes in contact with a resistive layer on the last float glass electrode; RPC2 had high voltage electrodes in direct contact with the last float glass electrode; both used 0.55 mm thick float glass resistive electrodes and had 2×7 140 μm gas gaps. RPC3 used 0.7 mm thick low-resistivity glass electrodes (2.5×10^{10} Ωcm) with 2×5 140 μm gas gaps and high voltage electrode strips in direct contact with the last glass electrode. All RPC structures were housed in gas-tight aluminum boxes.
In-beam tests of RPC1, RPC2, and RPC3 were conducted at CERN-PS's T10 beam line using a 6 GeV/c pion beam. A photo of the experimental setup is presented in Fig.15. For some runs, one RPC was positioned orthogonally to the other two in order to estimate position resolution along the strips, allowing

to condition the horizontal strip positions by requiring coincidence with hits on the vertical strips of the non-rotated RPC (Fig.16). Signals from both ends of the RPC strips were amplified and discriminated by NINO-based differential front-end electronics.

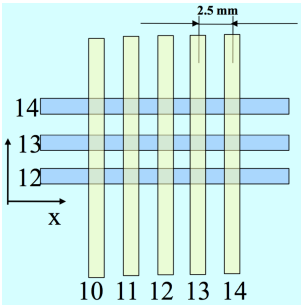

Figure 16

Time and Time-over-Threshold (ToT) signals from both sides of 15 strips of each counter were recorded. Two pairs of plastic scintillators with 1×1 cm^2 overlap served as active collimators, and two plastic scintillators read out at both ends (2×2 cm^2 overlap) were used as time references. Two TDC channels recorded signals from both ends of a reference plastic scintillator.

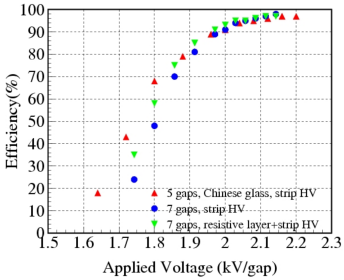

Figure 17

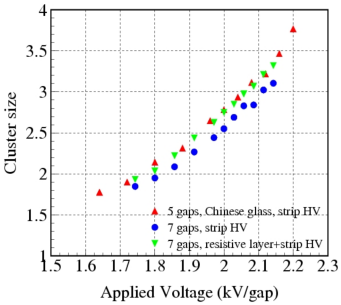

Figure 18

Three different gas mixtures were tested: 85% $C_2F_4H_2$ + 5% SF_6 + 10% iso-C_4H_{10}, 90% $C_2F_4H_2$ + 5% SF_6 + 5% iso-C_4H_{10}, and 95% $C_2F_4H_2$ + 5% SF_6. The efficiency of each RPC was calculated as the number of events with hits providing valid time and ToT information at both ends of the operated strips, divided by the number of triggers. The results are presented in Fig. 17.
At lower voltages, before reaching the efficiency plateau, RPC3, based on low resistivity glass (2.5×10^{10} Ωcm), exhibited higher efficiency compared to RPC1, which uses float glass (4×10^{12} Ωcm) with high voltage electrode strips in contact with a resistive layer applied on the last glass electrode. RPC2, where the

high voltage strips are in direct contact with the glass electrode, showed the lowest efficiency. However, at 2.1 kV/gap, all prototypes achieved an efficiency of approximately 97%.
The cluster size as a function of the applied voltage per gap is shown in Fig.18 for the three RPCs. RPC2, in which the high voltage electrode strips are in direct contact with the float glass electrodes, consistently displayed a lower cluster size by about 0.25 strips. At approximately 2.1 kV/gap, where efficiency exceeds 95%, the cluster size is around 3 strips, corresponding to 7.5 mm.

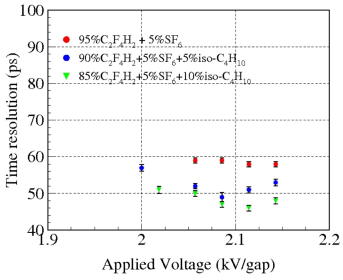

Figure 19

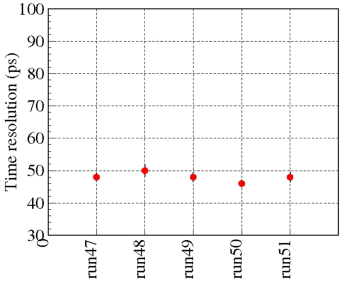

Figure 20

The time resolution was estimated using plastic scintillators as the reference time or by measuring the time difference between two RPCs, assuming they have the same time resolution. Fig.19 presents the time resolution of RPC1 as a function of the applied voltage for the three gas mixtures, using the plastic scintillator as the reference time. The addition of isobutane improved the time resolution by approximately 15%, achieving a resolution better than 50 ps at 2.1 kV/gap. This improvement can be attributed to the higher primary ionization in isobutane.
Fig.20 shows the time resolution for different runs using the time difference between RPC3 and RPC2, confirming the previous results. Considering that these runs were conducted over a period of 6 hours, this result also confirms the stability of the counters, gas flow, and electronics.
Each strip is read out at both ends, allowing access to the position information along the strip using the time difference. To extract the resolution, we selected tracks collimated within a strip pitch (2.54 mm) of the non-rotated RPC prototype, as schematically presented in Fig.16. The obtained position resolution along the strip direction is shown in Fig.21 for two strips of the RPC rotated by 90°, using the condition on five orthogonal strips of the reference counter. A position resolution of approximately 4.5 mm was achieved.
The position information across the strips was obtained using the runs where all three prototypes had the same orientation. The result for RPC3, using the residuals distribution relative to the track reconstructed with the position information of all three counters, is presented in Fig.22. The hit position in each counter was determined using a Gaussian Pad Response Function. The position resolution depends on the type of glass and the method of applying the high voltage, either

directly on the glass electrodes or via a resistive layer. This resolution ranges from 220 μm to 450 μm.

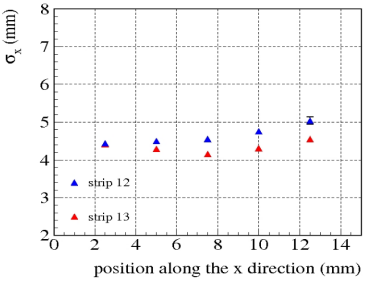

Figure 21

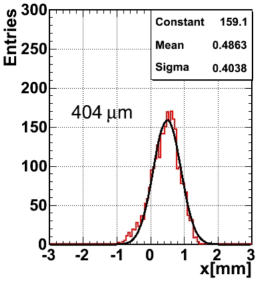

Figure 22

The RPCs were operated at 2.1 kV/gap. As shown in Fig.22, RPC3, which is based on low resistivity glass electrodes, achieves a position resolution across the strips of about 400 μm. These results obtained with the RPC1, RPC2, and RPC3 prototypes in terms of time resolution and position resolution along and across the strips are excellent. However, the number of channels required to fully equip such MSMGRPC is relatively high. In order to reduce the cost, a new prototype (RPC4) was designed and built. The strip structure of the electrodes has a 7.112 mm pitch (5.588 mm strip width and 1.524 mm space between strips) and 96 mm length. The RPC active area of 96×280 mm^2 is covered by 40 strips. Two such prototypes (RPC4a and RPC4b) were constructed using low resistivity glass electrodes of 0.7 mm thickness and 2×5 140 μm gas gaps. These were staggered, with an overlap of 6 mm along the strips, as shown in Fig.23, and placed in the same tight gas box.

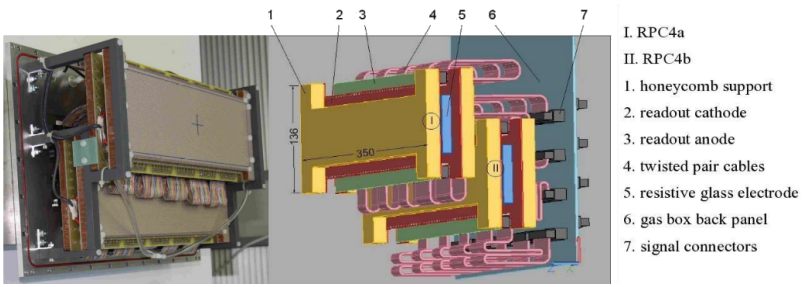

Figure 23

High counting rate tests were performed at Jülich-COSY with a proton beam of 2.5 GeV/c. The beam intensity ranged from 10^4 to 10^6 protons/s. A new motherboard version, featuring an 8-channel NINO chip bonded on it and housed by a front-end board designed by our group, was used for signal processing. This highly integrated

front-end electronics was mounted on the backplane of the housing box. Signals from 64 strips read out at both ends were recorded. In addition to the new RPC4 prototypes (based on the two RPC cells with a 7.112 mm strip pitch), RPC3 was also installed in the beamline as a time reference.
The RPCs were flushed with an 85% $C_2F_4H_2$+10% SF_6+5% iso-C_4H_{10} gas mixture. The LVDS-NINO outputs were sent to 32-channel V1290A CAEN TDCs. ToT information delivered by the NINO chip was used for slewing correction and position information across the strips.

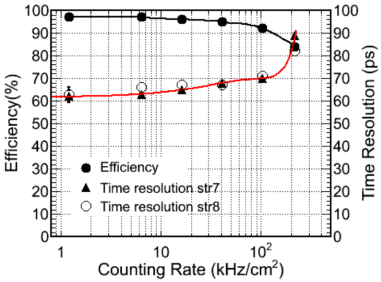

Figure 24

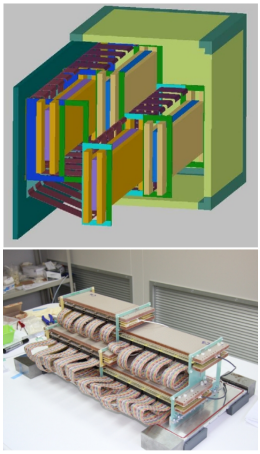

Figure 25

The performance of the 7.112 mm pitch prototype, featuring two overlapping cells, is illustrated in Fig.24. The time resolution is derived from the time difference between the overlapping zones of RPC4a and RPC4b, indicated by full triangles. The efficiency, using RPC3 as the reference counter, is depicted by full dots. Even at a rate of 100,000 particles/cm^2 · sec, the time resolution remains below 70 ps and the efficiency above 90% [M. Petrovici et al., JINST7(2012)P11003; M. Petris and M. Petrovici, Jour. of Physics: Conf. Series 533(2014)012009].
Due to the size constraints of low resistivity glass electrodes, a continuous coverage of a large surface can be achieved by staggering MSMGRPCs not only along the strips, as previously shown, but also across the strips. This design is presented in Fig.25. Four MSMGRPCs are staggered along (16.5 mm overlap) and across (17.5 mm overlap) the read-out strips and housed inside a gas-tight box. The structure of the RPC cells is identical to the one previously described. The gas box is constructed with honeycomb sheets (10 mm) sandwiched between two Stesalit layers (0.4 mm), plated on the inner side with a 0.13 mm copper layer. The back plate is made of 12 mm thick aluminum, supporting the RPC cells. PCB plates with connectors are glued onto machined rectangular openings for signal transmission from the RPC cells to the front-end electronics.
The beam test was conducted at the T9 beam line of the CERN PS accelerator using a mixed electron and pion beam with momenta of 2-8 GeV/c. Fig.26 shows

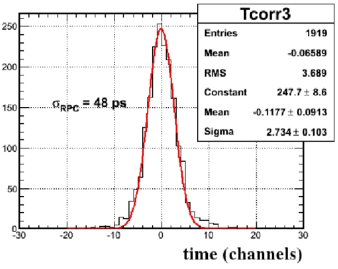

Figure 26

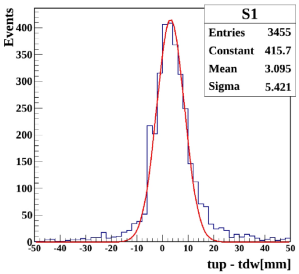

Figure 27

a time resolution of 48 ps for the overlapping zone along the strips of two MGMS-RPC cells, after walk correction, including electronics contributions. The position resolution along the strip, shown in Fig.27, is 5.4 mm, derived from the calibrated time difference measured at both strip ends, using position information from a narrow strip reference RPC [M.Petris et al., CBM Progress Report 2012, pg.68].

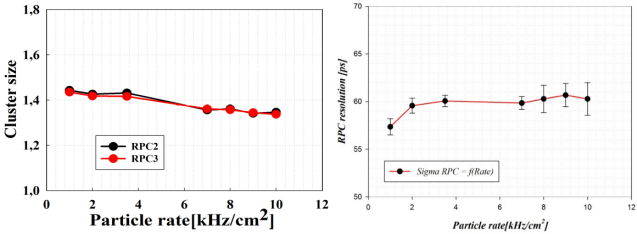

Figure 28

The same structure was tested at the SIS18 accelerator of GSI-Darmstadt with charged particles produced by colliding 1.7A·GeV Ni ions with a 1 mm thick Pb-target, at the highest intensity per spill delivered by SIS18. The detector was operated with a gas mixture of 85% $C_2F_4H_2$+10% SF_6+5% iso-C_4H_{10}, at an electric field strength of 157 kV/cm. Signals from 16 strips of each cell were processed by NINO fast amplifiers, with differential outputs converted by FPGA TDCs [J.Fruhauf et al., CBM Progress Report 2012, p.71].

Fig.28 shows the cluster size and time resolution as a function of particle rate, demonstrating excellent performance up to 10 kHz/sec·cm^2, the highest accessible rate at that time at SIS18 [A. Balaceanu et al., CBM Progress Report 2013, pg. 78; M. Petris et al., Journal of Physics: Conference Series 724(2016)012037].

For applications requiring less granularity and a 100 Ω impedance transmission line, a new prototype with a 4.19 mm strip pitch, 2.16 mm strip width, 200 mm strip length, and an active area of 283×200 mm^2 using low resistivity glass electrodes was developed, as shown in Fig.29. The strip configuration was determined using APLAC simulation (Fig.30).

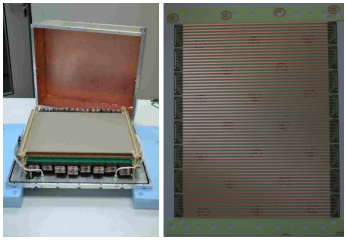

Figure 29

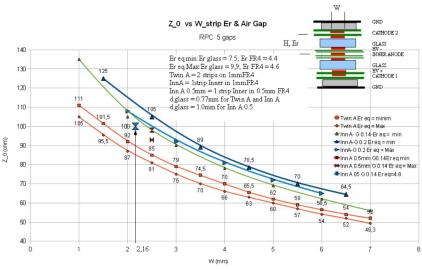

Figure 30

This prototype was operated at 2×5.5 kV with a gas mixture of 85% $C_2F_4H_2$+10% SF_6+5% iso-C_4H_{10}. In-house cosmic ray tests were followed by in-beam tests at SIS18 GSI-Darmstadt and CERN-PS. For both in-house and PS-CERN measurements, strip signals were processed by NINO chips, with differential outputs converted by CAEN V1290A TDCs.

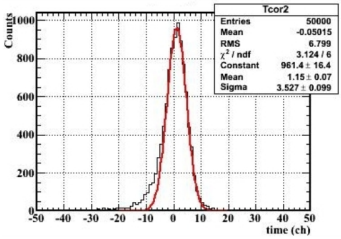

Figure 31

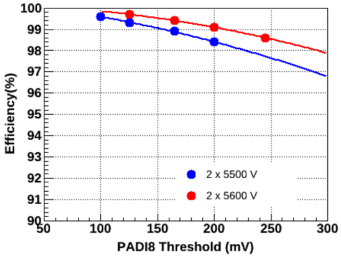

Figure 32

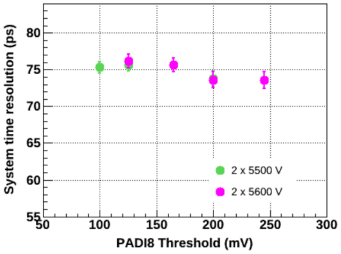

Figure 33

A typical time spectrum is presented in Fig.31. The in-beam test at SIS18 focused on compatibility with the new PADI8 FEE, designed for the CBM-TOF wall [M. Ciobanu et al., IEEE TNS, Vol.61, No. 2, pp.1015-1023, 2014]. The MGMSRPC signals were converted by FPGA TDCs. The efficiency as a function of the PADI8 thresholds for two applied high voltages (±5.5 kV and ±5.6 kV), corresponding to 157 kV/cm and 160 kV/cm electric field respectively, is shown in Fig.32. Fig.33

presents the system time resolution for each PADI8 threshold value, showing a slight improvement with increasing thresholds, with the best value being approximately 74 ps, including electronics contributions [M. Petris et al., CBM Progress Report 2014, pg. 95; M.Petris et al., JINST 11(2016)C09009].

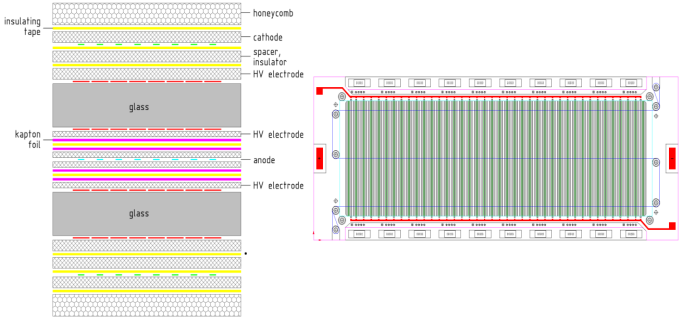

Figure 34

For the free-streaming readout experiment, achieving a good impedance match between the counters and the front-end electronics is crucial in order to minimise reflections on the transmission lines. For strip RPCs, this is challenging due to the imposed width of the transmission line and the electrode-gaps architecture, dictated by both physics and cost considerations. A new MGMSRPC prototype was designed to match the input impedance of the front-end electronics using an innovative idea, by adjusting the readout strip width, different from that of the high voltage (HV) electrodes. The new MSMGRPC architecture with impedance matched to the front-end electronics is presented in Fig.34.

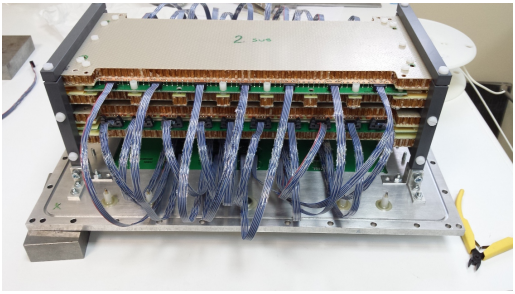

Figure 35

A strip pitch of 7.2 mm was selected, yielding an average cluster size of 1.5 strips as of the previous prototypes for the same inner geometry (2×5 gas gaps). The 5.6 mm strip width of the HV electrodes defines the counter granularity, while the 1.3 mm strip width of the readout electrodes defines the transmission line impedance of 100 Ω. Single-sided (8 gas gaps of 140 μm each, 10.1 mm strip pitch = 8.6 mm

width + 1.5 mm gap) and double-sided (2×5 gas gaps of 140 μm each, 7.2 mm strip pitch = 5.9 mm width + 1.3 mm gap) prototypes with these structures were built and assembled in a common gas-tight housing box (Fig.35.). Both prototypes used low resistivity glass electrodes of 0.7 mm. Signals were amplified by PADIX fast amplifiers, converted and processed by FPGA TDCs and TRB3 [M. Traxler et al, GSI Scientific Report 2014(2015)pg.514]. Each prototype had an active area of 96×300 mm^2.

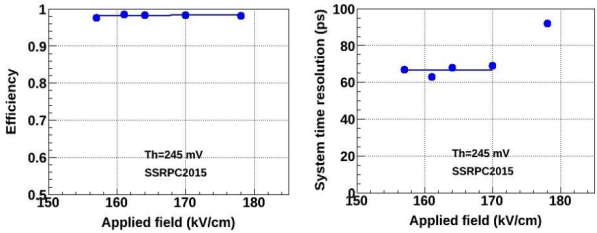

Figure 36

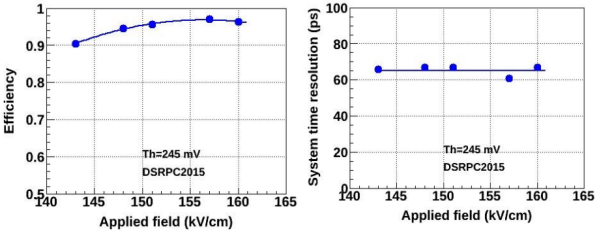

Figure 37

The efficiency and time resolution of single and double-sided prototypes using charged particles produced by a Pb projectile of 30 A·GeV on a Pb target at CERN-SPS are shown in Fig.36 and Fig.37, respectively. A system time resolution of 67 ps was achieved, with the efficiency plateau reaching 97%-98%. Long-term stability tests demonstrated excellent performance, as shown in Fig.38 and Fig.39 for single-sided and double-sided MSMGRPCs, respectively. The efficiency remained constant at about 97% for 10 hours of exposure, and the system time resolution improved by approximately 5 ps due to a conditioning process [M. Petris et al., CBM Progress Report 2015, pg. 97; V. Aprodu et al., CBM Progress Report 2015, pg. 98; M. Petris et al., CBM Progress Report 2016, pg. 131].

The prototypes were also tested in-beam at CERN-SPS with reaction products produced by a primary Pb beam with momenta of 13 A·GeV, 30 A·GeV, and 150 A·GeV incident on a Pb target. For the first time in an in-beam test of the CBM-TOF group, signal processing and readout were performed by a free-streaming DAQ system equipped with GET4-TDC [https://wiki.gsi.de/pub/EE/GeT4/

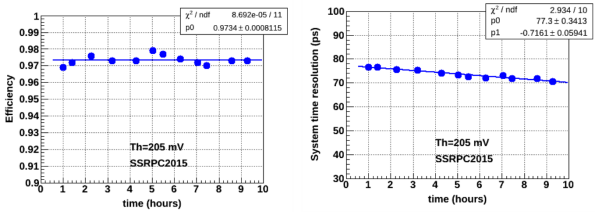

Figure 38

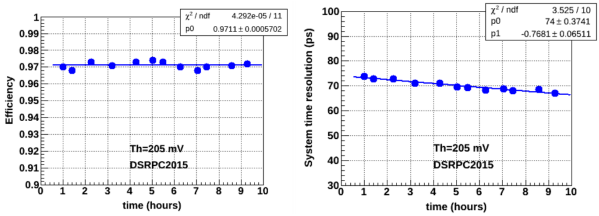

Figure 39

get4.pdf], using AFCK with gDPB firmware developed at GSI and Heidelberg, Germany. A very good system time resolution of 62 ps, including electronics contribution, was achieved for both MSMGRPCs operating at 157 kV/cm, with the PADIX threshold set to 200 mV. Assuming equal contributions from both counters, a single counter resolution of 44 ps was obtained. The efficiency ranged from 91.5% to 93.4%, depending on the hit selection based on window correlation of x and y coordinates in the two detectors [M. Petris et al., CBM Progress Report 2017, pg. 110].

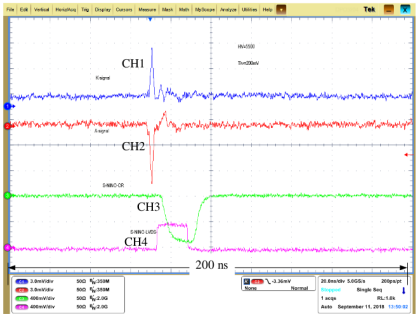

Figure 40

To establish a modulo 8 strip structure, given the fast amplifiers with 8 channels and the full length of the low resistivity glass electrodes, two MGMSRPC prototypes with 32 readout strips were designed and built. These prototypes feature

an inner architecture similar to the previously described prototypes. The readout strip width of 1.27 mm corresponds to a 100 Ω characteristic impedance of the differential transmission line, given a high voltage electrode strip width of 7.37 mm and a pitch of 9.02 mm. The detector was operated with a standard gas mixture at 2×5.5 kV.
A snapshot of the signals produced by cosmic rays from both cathode (CH1) and anode (CH2) readout strips, recorded directly from the detector at one end of the strip, and the output of the NINO FEE, i.e., the LVDS signal (CH4) and the logic OR (CH3), recorded at the other end, is presented in Fig.40. No reflections were observed on a 200 ns time scale (20 ns/div) [D. Bartos et al., Rom.Journ.Phys. 63(2018)901; M. Petris et al., CBM Progress Report 2018, pg.97].

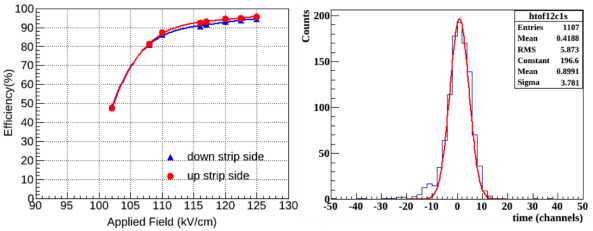

Figure 41

The prototypes were tested with reaction products (1.6 A·GeV 10^7Ag beam incident on a Au target) in the mCBM test setup at SIS18, GSI-Darmstadt. The signals delivered by the detectors were processed by PADIX FEE and a free streaming DAQ equipped with GET4-TDCs, yielding a single counter time resolution of 55 ps, including electronics chain contribution. Similar to previous prototypes, a lower efficiency was observed with the free streaming readout chain compared to laboratory tests using NINO fast amplifiers. This difference was attributed to the lower gain of the PADI amplifiers [M. Petris et al., CBM Progress Report 2019, pg.131; V. Aprodu et al., CBM Progress Report 2019, pg.132; M. Petris et al., NIM A 920 (2019), 100].

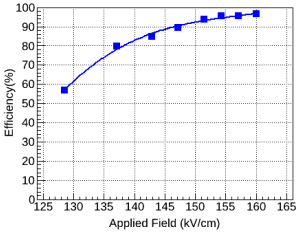

Figure 42

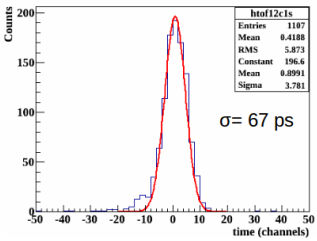

Figure 43

To address this issue, two new MSMGRPC prototypes with an increased gap size of 200 μm, maintaining the same inner geometry and architecture for the high

voltage and readout electrodes, were assembled. Using a ^{60}Co source and an array of collimators in a Pb plate in front of the detector, a uniform detection efficiency over the full length of the strip and a single counter time resolution of about 67 ps were obtained (Fig.41). Based on the peaks' positions in the yield distributions, corresponding to a 5.6 cm distance between the outermost collimators and the 0.025 ns/ch TDC calibration, a signal propagation velocity of 16 cm/ns was determined.
Cosmic ray tests conducted in Heidelberg confirmed that the lower efficiency was due to the low gain of PADIX. The efficiency and time resolution results are shown in Fig.42 and Fig.43. Comparisons of two PADI amplifier versions, X and X1, and our prototypes of 140 μm and 200 μm are detailed in Table 2.1 [I. Deppner et al., private communication].

Table 2.1: Efficiency Bucharest counter.

Efficiency	Gap 140 µm	Gap200 µm
PADI X	81%	93%
PAD X1	91%	98%

Equipped with the front-end electronics designed for the inner zone of CBM-TOF, integrating PADI X1 FEE and GET4 TDCs on the same motherboard, the counters operated with a gas mixture of 97.5% $C_2H_2F_4$ + 2.5% SF_6 were tested in the mCBM experimental setup at SIS18 using a 2 A $\cdot$ GeV ^{16}O beam on a Au target. The results, including efficiency, time resolution, and time resolution as a function of counting rate, are shown in Fig.44 [M. Petris et al., CBM Progress Report 2021, pg.127].

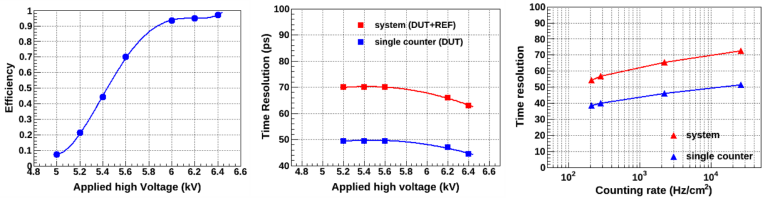

Figure 44

The CBM experiment is planned to operate at interaction rates up to 10^7 events/sec for Au-Au collisions at $\sqrt{s_{NN}} = 2-5$ GeV, over two months per year for ten years. Thus, all CBM components must be tested to ensure that the ageing effects do not deteriorate performance over the equipment's expected lifetime. We initiated ageing tests of MSMGRPC prototypes based on low resistivity glass electrodes using a 360 kCi ^{60}Co source at the Multipurpose Irradiation Facility (IRASM) of IFIN-HH, Bucharest. The two MSMGRPCs shown in Fig.35 were mounted in the IRASM cave, with only the double-sided prototype operated during irradiation. After successive exposures, in total 40 hours, a charge of 0.127 C/cm^2 was accumulated. Post-exposure, detailed tests were conducted in our laboratory using NINO front-end electronics and V1290A CAEN TDCs.

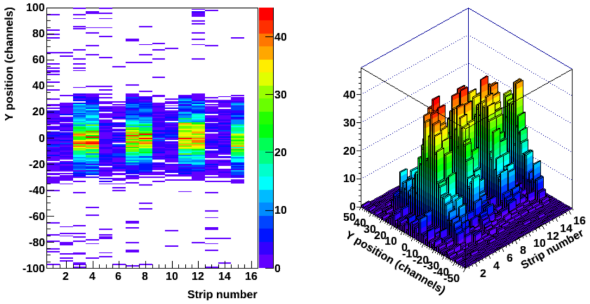

Figure 45

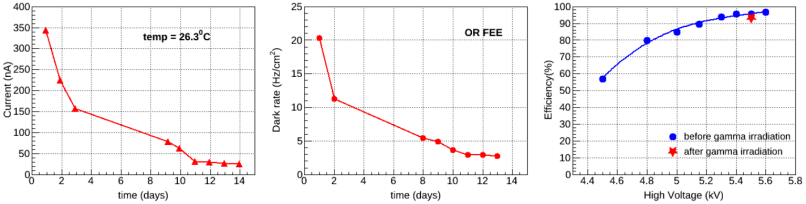

Figure 46

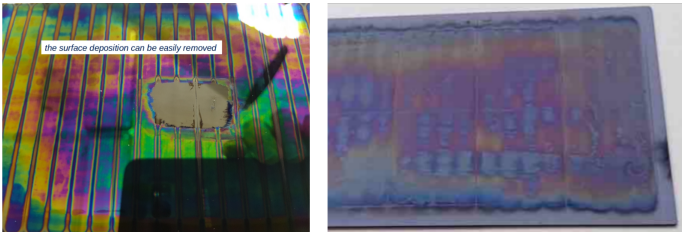

Figure 47

In self-trigger mode operation, the counting rate as a function of strip number and position along the strips showed increased activity near the spacers (Fig.45). Two weeks post-exposure, the dark current and rate decreased to pre-exposure values, with efficiency returning to baseline as shown in Fig.46. Various depositions on the glass electrodes' surfaces were evidenced after disassembling the detector. The cathode-facing side exhibited thick, removable deposits, while the anode-facing side had more attenuated, less removable deposits (Fig.47). The deposited layers could be cleaned with ethyl alcohol, and regular patterns due to ablation/etching were observed on the anode-facing side.

The deposited layers' composition and properties were analyzed using SEM, XPS, foil-ERDA, RBS, AFM, and THz-TDS techniques, confirming earlier studies on ablation and polymerization in low-pressure plasma or moderate irradiation doses. [D. Bartos et al., NIM A1024(2022)166122].

Deposition of different radicals produced by polymerisation on the surface of the floating glass electrodes facing the cathode electrode, with relative weights of different elements as a function of deepness of the deposited layer is evidenced. These layers could be easily cleaned using ethyl alcohol. Fluorine radicals which produce ablation/etching of the surface of glass electrodes facing the anode is evidenced. Besides a continuous layer, regular patterns are evidenced which could be explained as the results of already existing tiny patterns on the non-exposed glass which are enhanced by ablation/etching process.

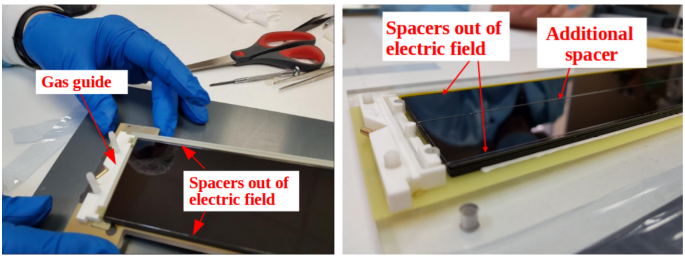

Figure 48

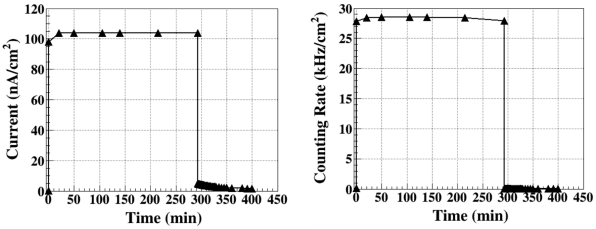

Figure 49

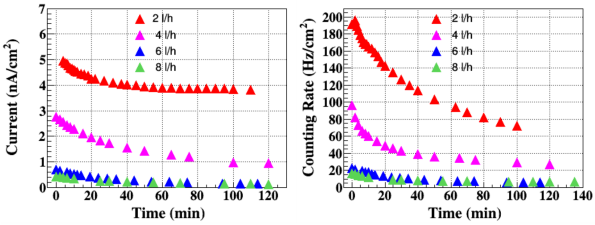

Figure 50

The surfaces roughness increases relative to the non-irradiated glass. Surface and volume resistivity, dark current, counting rate, efficiency and cluster size measurements after irradiation show that there is a recovery process which brings the counter to the initial performance before the irradiation. The present studies summarized above were performed using a housing box flashed by the gas mixture.

Therefore the gas exchange in the 140 μm 10 gas gaps of the counter was via diffusion. It is well known that the polymerisation phenomenon is inverse proportional with the gas flow. Therefore, a directed gas flow through the gas gaps is expected to decrease the observed ageing process. A new MSMGRPC prototype, with 70% direct gas flow through the gaps was designed and assembled. The architecture is similar with the one of the previous prototypes. It was tested also in-beam within mCBM at SIS18. The obtained efficiency dependence on HV and time resolution were the same as for the previous MSMGRPC operated in a diffusion mode [V. Aprodu et al. CBM Progress Report 2021, pg.131].
A prototype with 100% gas transmission through the gaps was assembled (Fig.48). Aging effects were studied using two Amptek mini-X ray tubes, illuminating the MSMGRPC surface at ≥ 20 kHz/cm^2. The detector was operated using 97.5% tetrafluoroethane and 2.5% SF_6. The exposure was conducted for 5-7 hours per day, monitoring current and counting rate (Fig.49). After irradiation measurements showed reduced irradiation effects at a 6 l/h gas flow rate (Fig.50).

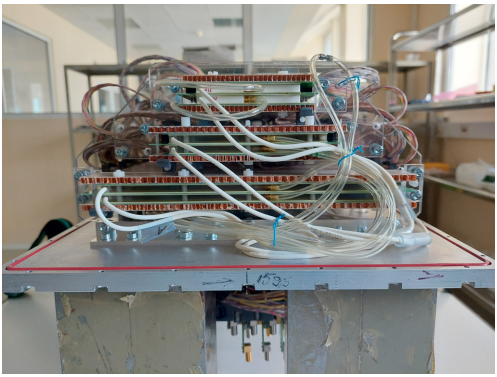

Figure 51

Two more prototypes with 100 mm and 200 mm strip lengths were assembled and underwent similar irradiation tests, yielding consistent results. The three prototypes, stacked one on top of each other, achieved about 95% efficiency and 60 ps time resolution in cosmic ray tests (Fig.51).
A mapping of the active area of the chambers in a self trigger mode operation of the DAQ system revealed an activity around the spacer positions. This can be seen in the two dimensional representation of the position along the strip versus strip number shown in Fig.52.
The position along the strip was obtained based on the time difference between the two ends of each strip.
From the Gauss fit of the two middle peaks seen in the one dimensional projection along one strip (Fig.52-right), an accuracy of the position determination along the strip of 4.5±0.1 mm was estimated. Based on the distance between the two middle peaks and the TDC calibration of 25 ps/bin, a 17 cm/ns signal propagation

velocity along the strip was determined. In order to minimise the ageing effects around the spacers, we reduced their size, replacing the continuous nylon fishing line by discrete pad spacers.

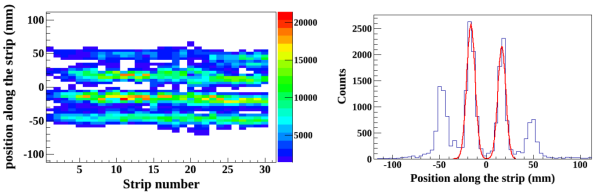

Figure 52

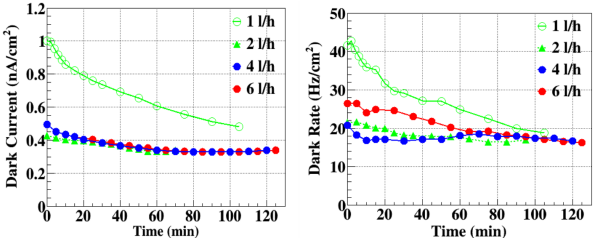

Figure 53

In a first step, we manufactured rectangular spacers of 2 mm × 2 mm size and 200 μm thickness, made of sticky polyimide (kapton type). Similar ageing tests using the 2 X-ray tubes, as for the previous direct flow prototypes based on fishing line spacers, were performed. The obtained results showed lower values of the dark current and dark counting rate, as well as a much less impact of the gas flow rate (varied between 1 l/h to 6 l/h) on these parameters, as can be seen in Fig.53. Between 2 l/h and 6 l/h gas flow rate it was not observed any difference, the recovery in terms of the dark current and dark counting rate being fast and converging towards similar values in a short time. Based on these positive results, we decreased the gas flow up to 1 l/h. The measurements showed still low values of the dark current and dark counting rate with the same fast recovery in time.

Being aware that squared obstacles in a fluid flow create the so called stagnation region after the obstacle we decided to produce one more prototype based on discrete disk type spacers. We found commercially available disk shape spacers of 2 mm diameter, made of polyimide (kapton type) with a maximum available thickness of 170 μm and assembled a new MSMGRPC prototype using such spacers. Having a smaller gap size, the counter was operated at 2×5.7 kV during the ageing tests.

The measured counting rate versus current for increasing fluxes of X-rays shows a very good linearity up to the maximum measured counting rate of 28 kHz/cm2 (Fig.54). For ageing effect investigations, the counter was exposed in successive days for 6 hours each day, measuring the dark current and dark counting rate

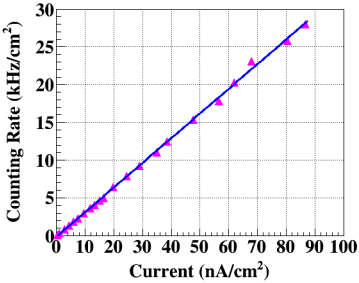

Figure 54

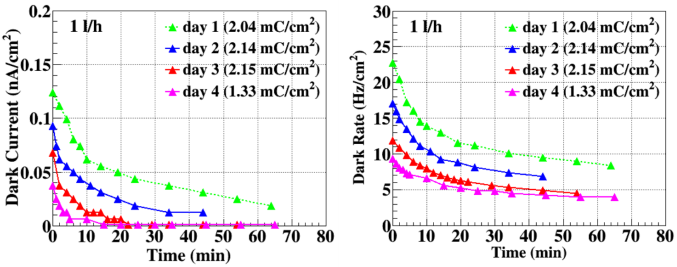

Figure 55

recovery in time after each exposure for 2 hours at 1 l/h gas flow rate. Fig.55 shows very low values of the dark current and dark counting rate after each exposure. A conditioning effect from one day to the other is observed. We reduced the gas flow rate to 0.5 l/h and exposed the chamber for the same time interval for one more day.

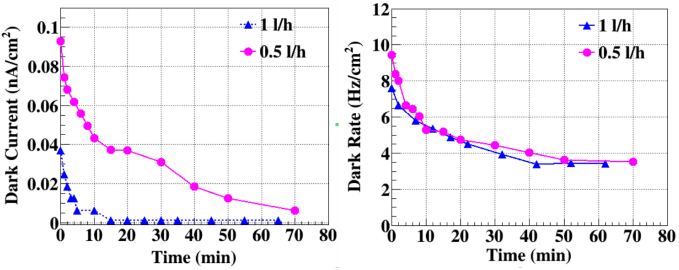

Figure 56

The results presented in Fig.56 show that the dark counting rate has very low values, without significant differences from the ones measured at 1 l/h gas flow rate.

Dedicated high counting rate tests using minimum ionization particles are in progress. However, the results obtained using high flux X-rays described above, i.e. the ageing effects in MSMGRPCs using direct flow through the gaps and discrete spacers relative to those obtained using direct flow and fishing line as spacers or even worse in the case of gas exchange in the gaps via diffusion will remain valid [M. Petris et al, NIM A1045(2023)167621; V. Aprodu et al., NIM A1049(2023), 168098; M.Petris et al., arXiv:2403.14190[physics.ins-det], in print at NIM].

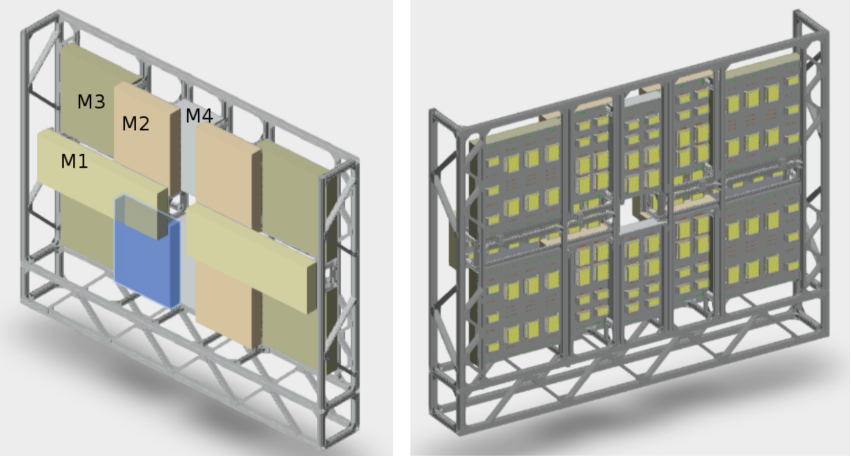

Figure 57

All these results substantiated the decision to recommend such type of MSMGRPCs as solution for the inner zone of the Time of Flight (ToF) wall of the CBM experiment at SIS100 - FAIR, Darmstadt.

A sketch of the CBM-ToF inner zone architecture in the support frame can be followed in Fig.57, left-front view, right-back view. The structure contains 12 modules of 4 types (M0, M1, M2, M3), staggered in z direction, such to obtain a continuous coverage of the active area. Inside a module the counters are staggered on four layers in z directions with a minimum overlap between them and continuous coverage of the active area, for a 8 m distance from the target. The 0.9 mm strip pitch is the same for all three counter types, their granularity being adjusted through the corresponding strip length of 60 mm (MRPC1a), 100 mm (MRPC1b) and 200 mm (MRPC1c).

As an example, in Fig.58 is presented the structure of one of the most complex modules, M0, in progress to be equipped with the three types of RPCs [V. Duta et al., CBM Progress Report 2019, pg.134].

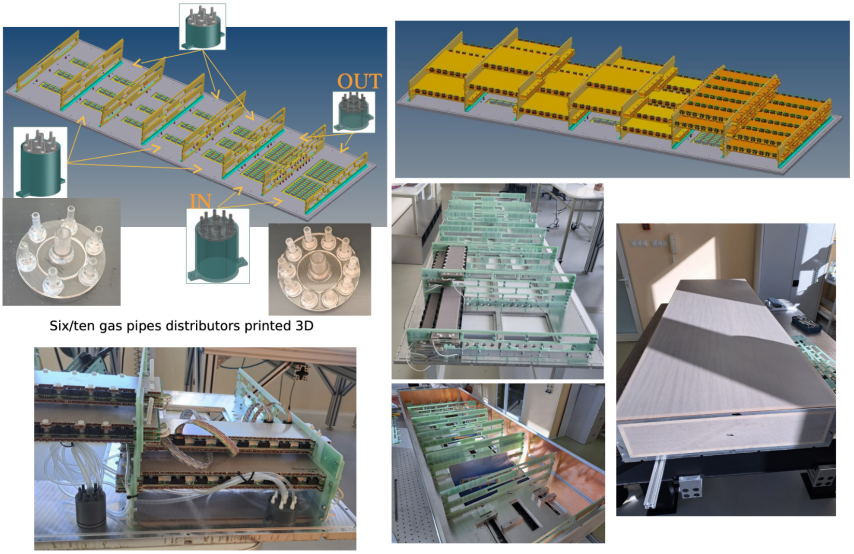

Figure 58

We are rather confident that FAIR Council will take the right decision to include CBM experiment in the "First Physics" stage of FAIR. Once this will be the case, the in-kind contract to realize the whole inner zone of the CBM-ToF subdetector will be sent for the corresponding signatures in order to access the financial support from Romania as a commitment to FAIR experiments.

TRDs

Transition Radiation Detectors (TRD) are essential for tracking and lepton identification in numerous experiments. Large area TRD detectors have been constructed for LHC experiments. One notable example is the Transition Radiation Tracker (TRT) of the ATLAS experiment, which is based on straw tubes and meets the requirement of maintaining its performance up to 10^7 particles per straw at moderate occupancies per event in pp collisions [ATLAS Collaboration, Inner Detector Technical Design Report, vols. I & II, CERN/LHCC/97-17 (1997)/hep-ex/0311058]. Another example is the ALICE TRD, which is based on multi-wire proportional chambers with a high-granularity readout electrode, designed to maintain performance up to the highest multiplicity anticipated in Pb-Pb collisions at LHC, with the counting rate limitation dictated by the 30 mm drift zone [ALICE-Collaboration, J. Phys. G30 (2004)1517].

Given these considerations, a natural solution for a fast TRD detector with high granularity, capable of handling high multiplicity and high interaction rates, is a Multiwire Proportional Chamber (MWPC) with a minimized drift region. This design achieves the necessary readout speed and reduces space charge effects. To achieve the desired occupancy per event, a pad readout electrode with corresponding granularity is required.
Our first prototype, shown in Fig. 59, had a symmetric structure with the anode wire plane located 3 mm from both the cathode and readout pad plane electrodes. The anode plane used 20 μm W-Au wires with a 2.5 mm pitch.

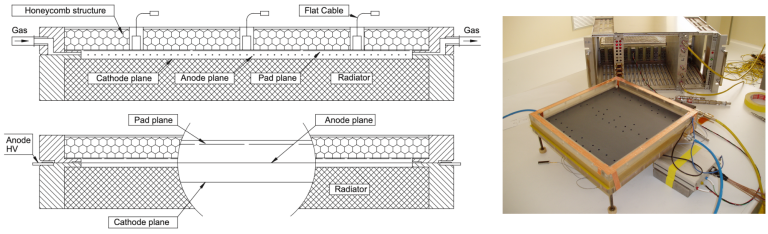

Figure 59

The pads were arranged in three rows along the anode wires, with each row containing 30 pads of approximately 7.5×80 mm^2 (width along the anode wire direction). The readout pad plane was reinforced with a honeycomb structure. The radiator (Rohacell foam HF71) supported the cathode plane, made of 25 μm aluminized mylar foil. The counter had an active area of 240×240 mm^2 [M. Petris et al., NIM A581(2007)406].

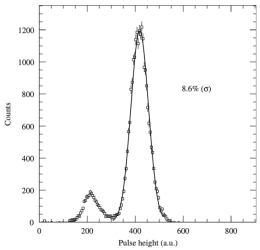

Figure 60

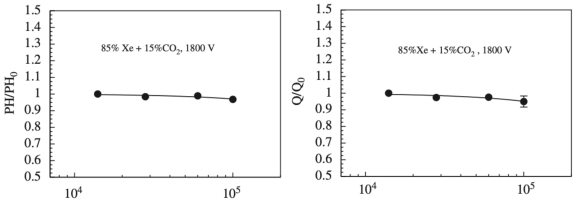

Figure 61

The pad signals were amplified by a custom-built charge-sensitive preamplifier shaper using discrete components, offering a gain of 2 mV/fC and noise of 1800 electrons rms. Charge or pulse height information was obtained by summing the sampled charge from the FADC converter (33 MHz sampling frequency) on the three consecutive pads in a row that fired during an event (the pad with maximum charge and its adjacent neighbours), to obtain the total deposited charge. The obtained energy resolution from the Gaussian fit of the main peak of the ^{55}Fe X-ray source was 8.6% (Fig.60). In-beam test results obtained, in a joint measurement campaign of the JRA4-I3HP Collaboration performed at the SIS18 accelerator of GSI-Darmstadt, in terms of the rate dependence of the maximum pulse height distribution and charge distribution for a Xe/CO_2 (85%/15%) gas mixture at 1800 V can be followed in Fig.61, and the position resolution as a function of the counting rate for different gas mixtures and applied voltages is presented in Fig. 62.

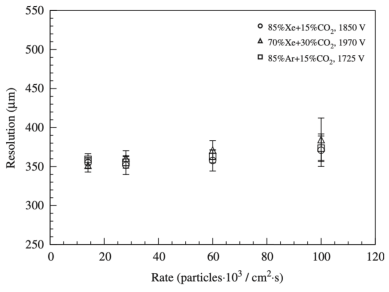

Figure 62

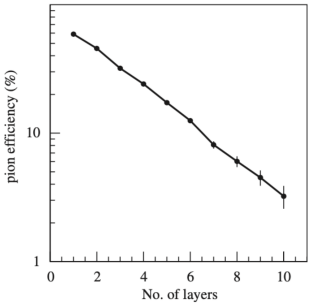

Figure 63

From a short run with negative particles (electrons and pions) of 1 GeV/c momentum, the pulse height distributions for electrons and pions were obtained summing the signals on the central and the adjacent pads. For the Rohacell HF71 radiator of the prototype, an anode voltage of 1900 V and a Xe/CO_2 (85%/15%) gas mixture, the pion efficiency at 90% electron efficiency can be followed in Fig.63 as a function of number of layers. The obtained pion efficiency for a configuration with ten layers was ∼3%. [M. Petris et al., NIM A581(2007)406].

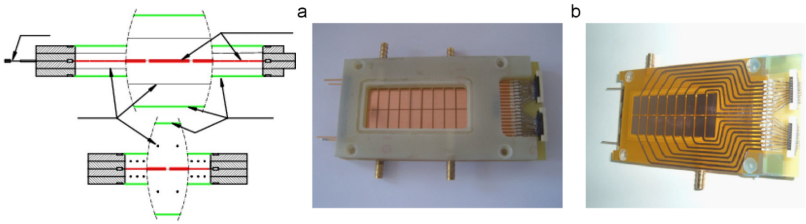

Figure 64

To achieve the same performance in high counting rate environments and higher pion rejection, we developed three versions of a new TRD prototype based on a double-sided pad readout electrode. The goal was to increase conversion efficiency while maintaining performance and the number of readout channels. This was achieved by symmetrising the counter structure relative to the readout electrode using a double-sided pad-plane electrode. The detector configuration and an assembled prototype are shown in Fig.64. The double-sided copper pad readout structure was etched on 25 μm kapton foil with evaporated copper. The measured X-ray absorption for this electrode was 1.5% at 5.9 keV.

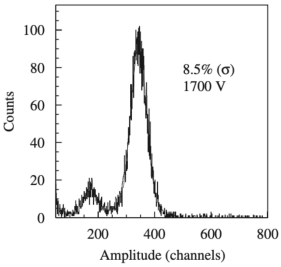

Figure 65

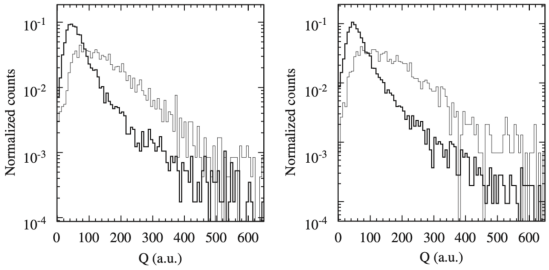

Figure 66

These prototypes were tested using a ^{55}Fe source, with signals processed by custom charge-sensitive preamplifier/shapers (gain: 2 mV/fC; noise: 1800 electrons rms) and digitized by an AD811 peak sensing ADC. The MBS GSI-type data acquisition system was used [H.G. Essel, N. Kurz, GSI Annual Report, 1998, pg.188]. Fig.65 shows a typical energy spectrum. In-beam tests, in a joint measurement campaign of the JRA4-I3HP Collaboration at SIS18, GSI-Darmstadt, demonstrated prototype performance with various gas mixtures, HV settings, momenta, and beam intensities. For all measurments a structure of fibers of 17 μm diameter of about 4.0 cm thickness and Rohacell HF71 of 2.0 cm thickness were used as radiator. Charge distributions of electrons (thin line) and pions (thick line) at 1.0 GeV/c and 1.5 GeV/c with a Xe/CO_2 (85%/15%) gas mixture and anode voltage of 1800 V are shown in Fig. 66.
Pion efficiency at 90% electron efficiency for 1.5 GeV/c as a function of the number

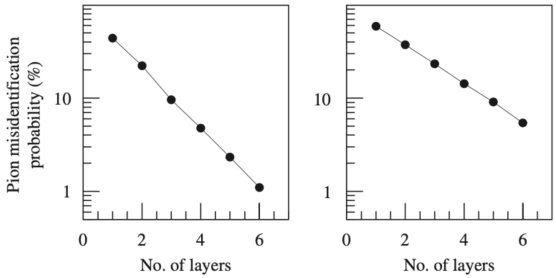

Figure 67

of layers for an anode voltage of 1700 V is shown in Fig. 67 for a stack of polypropylene foils with a regular periodic structure 20/500/120 (left) and Rohacell radiator (right). For the regularly spaced radiator an efficiency of 1.1% was obtained for a six layer structure. The most probable values of the Landau fit of the pulse height and charge distributions as a function of counting rate are presented Fig.68. Up to a counting rate of more than 2×10^5 particles/cm^{2}s virtually no deterioration of these values was observed [M. Petrovici et al., NIM A579(2007)961; M. Klein-Bosing et al, NIM A583(2008)83; M. Petris et al., Rom.Journ.Phys. 3(2010)324].

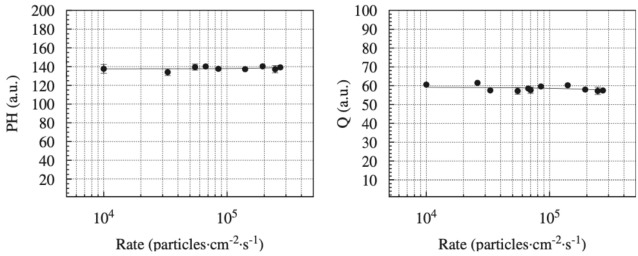

Figure 68

Although highly performant in terms of electron-pion rejection in high counting rate environment the size of these prototypes are too small to provide a reasonable geometrical efficiency for an large array. Therefore, a larger size prototype, using the same architecture, had to be developed. This can be achieved by increasing the sizes of the rectangular pads of the central double sided read-out electrode. Obviously, this conflicts with the requirements of high granularity and position resolution. In order to cope with this, each rectangular pad of 10×80 mm^2 was split on diagonal, each triangle being readout separately, see Fig.69. This choice of triangular-pad geometry of the read-out electrode allows for position determination in both coordinates: across and along the pads, respectively, as it is sketched in Fig.70.

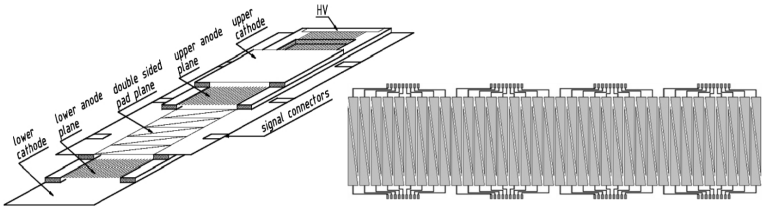

Figure 69

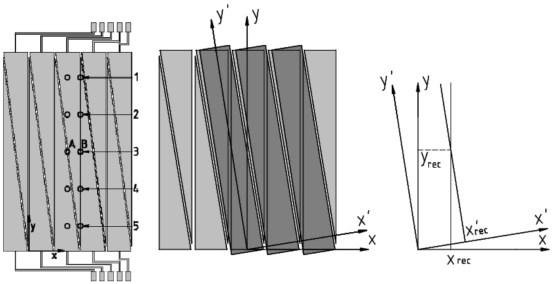

Figure 70

In parallel with these activities, an ASIC chip was designed in AMS CMOS 0.35 μm N-well technology (Fig.71). It has 8 identical analog channels, each with two outputs: one fast semi-Gaussian output and the other a peak-sense output (Fig.72). All channels have a self trigger capability with variable threshold. For an easy interconnection with an acquisition system, the chip implements an Input/Output interface working on a request/grant basis. There are also some specific features for high counting rate requirements: fast recovery from overload, good response to double pulse and high rate pulses, base line restoration due to leakage current and/or high counting rate. For testing purposes a test pulse generator was implemented at the chip level.

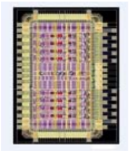

Figure 71

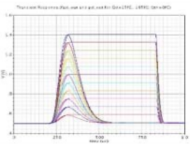

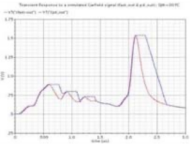

Figure 72

Tests with a collimated ^{238}Pu source achieved a position resolution of 0.97 mm across and 2.31 mm along the strips [V.Catanescu, "Specific requirements for analog electronics for a high counting rate TRD", CBM 10th Collaboration Meeting,

Sept.25-28, 2007, Dresden; V .Catanescu, D.Bartos, Gh.Caragheorgheopol, "Analog FEE for High Counting Rate Transition Radiation Detector", NuPECC, Bochum, March 18, 2009; V. Catanescu et al., CBM Progress Report 2009, pg. 47; M. Petrovici et al., Rom. Journ. Phys. 5-6(2011)654; M. Petris et al, NIM A714 (2013)17].

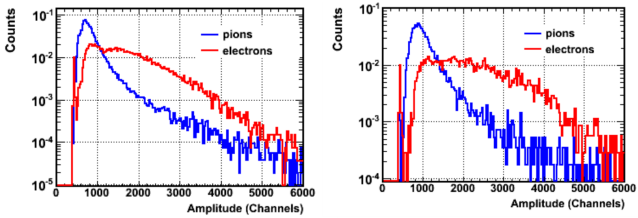

Figure 73

Two such prototypes, one with 4×3 mm distance between electrodes (V1) and the other with 4×4 mm (V2), were tested with a mixed electron/pion beam of 1-5 GeV/c momenta at T10 beam line of the CERN PS accelerator in a joint measurement campaign of the CBM Collaboration. TRD-V1 was operated at 1700 V with a regular radiator of the type 20/250/220 (i.e. 20 μm foil thickness, 250 μm gap, 220 foils), while TRD-V2 was operated at 2000 V with a regular radiator of the type 20/500/120, both being flashed with 80%/20% Xe/CO_2 gas mixture. Energy loss spectra for 2 GeV/c electrons (red line) and pions (blue line) measured with these two prototypes using regular radiator are presented in Fig.73 for 4×3 mm and 4×4 mm prototypes, respectively. Pion efficiency as a function of the number of TRD layers for 90% electron efficiency are shown in Fig.74. A 0.5% value was reached for a six TRD (4×4) layers. A position resolution across the pads of 327 μm and 6.3 mm along the pads was obtained [M. Petris et al., NIM A732 (2013) 375].

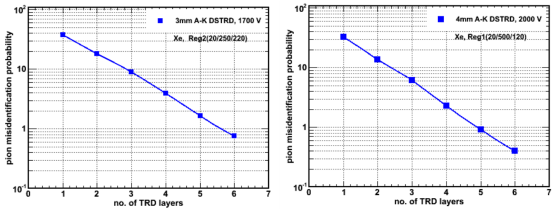

Figure 74

Although the previous prototypes demonstrated excellent e/π discrimination in a high counting rate environment, the size of a double-sided TRD is limited by the

topology of the signal routing. To address this issue, we developed a standard TRD architecture featuring a 2×4 mm amplification region coupled with a 4 mm drift zone. This design maintains the gas thickness identical to the 4×3 mm double-sided prototype, which exhibited very good performance. The drift zone size was optimized to minimize the drift time (less than 250 ns for an 80%Xe+20%CO_2 gas mixture, 2000 V anode voltage, and 500 V drift voltage), while maximizing the TR conversion efficiency. Details of this architecture are shown in Fig.75.

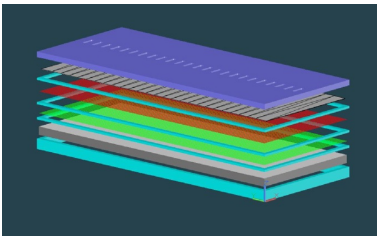

Figure 75

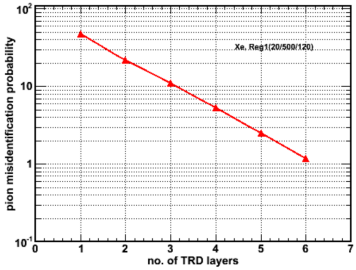

Figure 76

The detector was enclosed on one side by a drift electrode made from 25 μm thick aluminized Kapton foil, stretched over an 8 mm Rohacell plate, and on the other side by a 300 μm thick PCB readout electrode. The anode wire plane, of Au-coated W wires with a 20 μm diameter and 3 mm pitch, was positioned in the middle of the amplification region. The cathode wire plane, made from a Cu/Be alloy with a 75 μm diameter and 1.5 mm pitch, separates the amplification region from the drift zone. Rectangular pads (10×80 mm^2), split diagonally to form triangular readout cells, are read out separately. The pad signals were processed using 8-channel FASP front-end electronics.

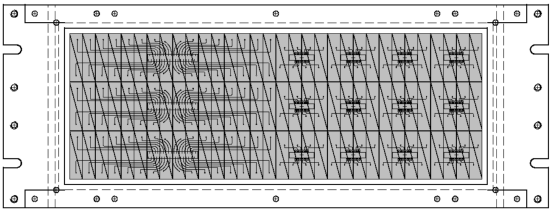

Figure 77

In-beam tests were conducted at the PS accelerator at CERN. The detector was operated with an 80%Xe+20%CO_2 gas mixture, 1900 V anode voltage, 400 V drift voltage, and a regular radiator of 20/500/120 (20 μm foil thickness, 500 μm gap, 120 foils). An electron misidentification probability of 1.1% was achieved for a 6-layer configuration, as shown in Fig.76, using pulse height distributions. Position

resolutions of approximately 320 μm across the pads and 6.3 mm along the pads were obtained [M. Petris et al., GSI Scientific Report 2011, pg.46].

Encouraged by these results, two identical prototypes for high multiplicity environments were designed and built. Each triangular pad had an area of approximately 1 cm^2 (2.7 cm height $\times$ 0.7 cm bottom width), as illustrated in Fig.77. For the ^{55}Fe source and in-beam tests, signals from 16 triangular pads (8 consecutive pads from two neighbouring rows) were processed by FASP using the flat-top output. A 32-channel peak sense Mesytec ADC (MADC-32) was used for digitisation. The detectors were tested with a mixed electron and pion beam of 2 - 10 GeV/c momenta at the T9 beam line of the CERN PS accelerator.
The pulse height distribution for pions (red colour) and electrons (blue colour) are presented in Fig.78 - left. A 1% pion misidentification probability was estimated for a configuration with seven TRD layers with a fibre radiator Fig.78 - right [M Petris et al., CBM Progress Report 2012, pg.59].

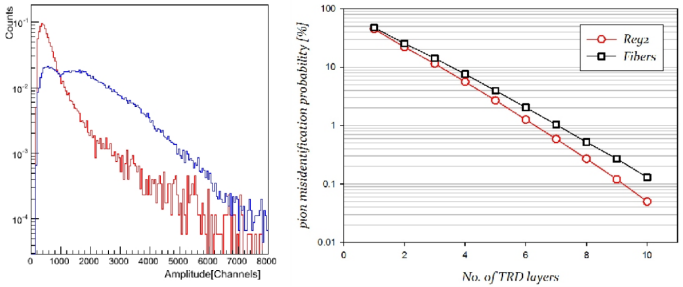

Figure 78

A new acquisition system for in-beam tests of the TRD prototypes was developed, featuring a free-running mode based on the Virtex-6 FPGA ML605 Evaluation Kit (Fig.79). The TRD signals, amplified by a FEE based on the FASP ASIC, were transmitted via a twisted pair cable to a fast ADC (MAX1434). This 10-bit analog-to-digital converter has fully differential inputs, a pipelined architecture, and digital error correction, supporting a maximum sample rate of 50 Msps.

The main tasks of the ML605 were:

- Clock generation,
- De-serialization of data from the MAX1434,
- Reading the synchronization signal from MBS,
- Ethernet communication.

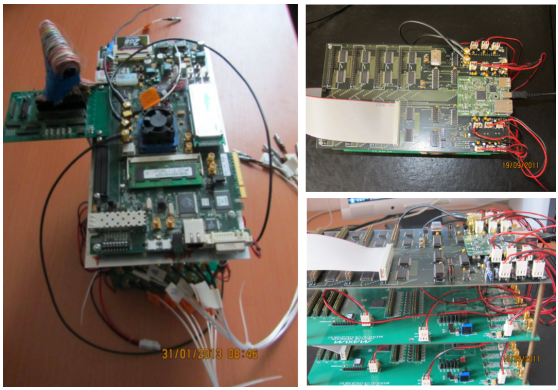

Figure 79

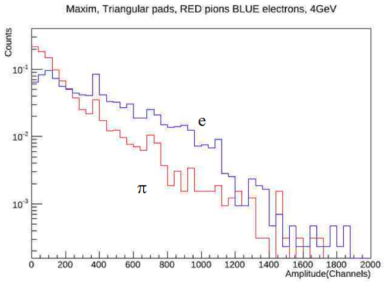

Figure 80

Fig.80 shows the electron-pion separation using a fibre radiator and a TRD prototype based on MWPC architecture with a 2×4 mm amplification zone and a 4 mm drift region. In-beam tests were conducted at the PS accelerator at CERN, where electrons and pions were selected using information from the Cherenkov detector and the lead glass calorimeter. Preliminary results indicated that the high counting rate prototypes developed for CBM, amplified by FASP, could be processed by the free-running mode architecture while maintaining their performance [F. Constantin and M. Petcu, CBM Progress Report 2011, pg.53; F. Constantin, CBM Progress Report 2012, pg.56].

Motivated by these results, a larger prototype, 539.8×557.8 mm^2, was assembled, with a 2×4 mm thick amplification region, a 4 mm thick drift zone, 3 mm anode pitch, and 1.5 mm cathode pitch. The pad plane comprises 9 columns and 20 rows, with 144 triangular pads per row, each of about 1 cm^2 area, individually read out. Signals from the pads are routed in groups of 16 and processed by the FASP FEE (Fig.81). This TRD prototype, along with smaller ones, were tested with a mixed electron-pion beam of 2-8 GeV/c momenta at the T9 beam line of the

CERN Proton Synchrotron. The chamber was flushed with an 80%Xe+20%CO_2 gas mixture and operated at 2000 V anode voltage and 800 V drift voltage.
As shown in Fig.82 - left, with a regular foil radiator of the type 20/250/220, a performance of about 1% in electron - pion discriminationwas estimated for a six-layer configuration. Fig.82 - right illustrates that the electron-pion separation performance is consistent across the detector surface.

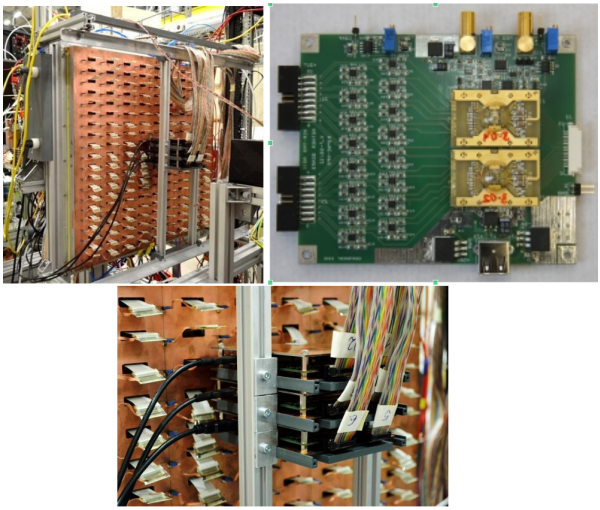

Figure 81

Using the information from all three prototypes delivered by the two types of triangular pad pairings (rectangular and tilted), it was demonstrated that the resolution along the pads is sufficient to identify the anode wire where the avalanche occurs (see Fig.83). In-beam tests showed a position resolution across the pads of approximately 385 μm and along the pads of approximately 1.6 mm [M Tarzila et al., CBM Progress Report 2012, pg.60; M. Tarzila et al., CBM Collaboration meeting, September 23-27, 2013, JINR, Dubna] .

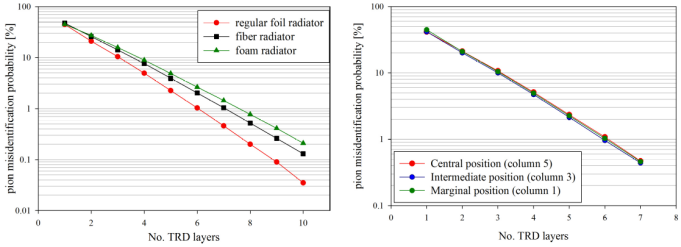

Figure 82

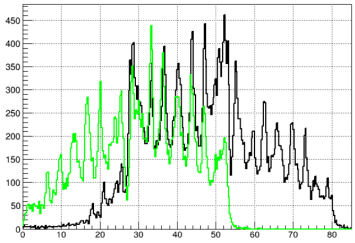

Figure 83

By implementing a Pad Response Function based on the position of the firing anode wire along the pads (ARF), using a ^{55}Fe source, the result presented in Fig.84 - left was obtained. The resolution of the ARF method was confirmed in in-beam tests at PS-CERN with minimum ionizing particles and a second TRD orthogonal to the first, using rectangular pairing of the triangular pads for good position resolution across pads. The correlation between position measurements in the reference detector and anode identification by ARF is shown in Fig.84 - right.

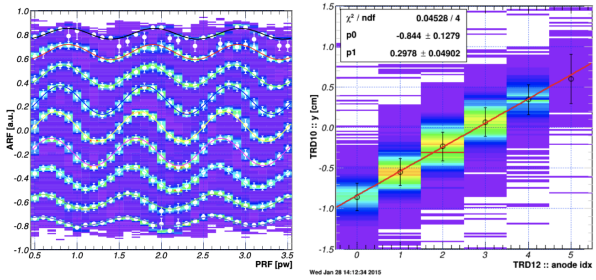

Figure 84

The measured distance of (2.98±0.05) mm between the anode wires agrees well with the designed pitch of 3 mm. Thus, it was demonstrated that using a triangular pad structure and varying PRF, good local anode identification can be achieved. This method opens the possibility of using reduced pad geometries, improving position resolution while maintaining constant read-out electronics cost and experimental material budget [A. Bercuci et al., CBM Progress report 2014, pg.81].

In the meantime, a second version of the FASP ASIC, dedicated to high counting rate TRDs developed by our group, was designed and produced. Similar to the first version, it is based on AMS 0.35 μm N-well technology. The die size is 4.65×3.45 mm^2 (Fig.85). In addition to the main features of its precursor, FASP-02 incorporates new features tailored to the fast TRD prototypes' specific architecture and test results.

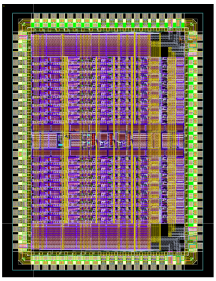

Figure 85

The most relevant new features are:

- 16 input channels;
- Selectable positive or negative polarity of the input signals;
- Multiplexed analog outputs, selectable between semi-Gaussian or flat top;
- Channel-wise clock synchronized logic time for individual ADCs;
- Channel-wise logic time signal generated at the selectable threshold level or at the signal peak detection, according to user settings;
- Selectable trigger of neighboring channels relative to the one with the signal above the threshold;
- Tilted and rectangular pairing of the triangular pads. [V. Catanescu, CBM Progress report 2014, pg.82.]

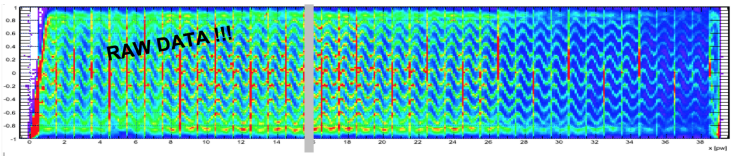

Figure 86

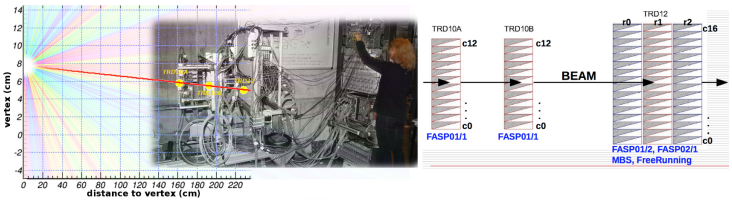

Figure 87

These results were confirmed in tests at SPS-CERN using reaction products from a 30 A·GeV Pb beam on a Pb target (Fig.86). Based on the three prototypes described above (Fig.87), the first tracking performance using such a 2D TRD architecture was performed, and the position of the target where the particles were produced was accurately reconstructed (Fig.88) [A. Bercuci et al, CBM Progress Report 2016, pg.121].

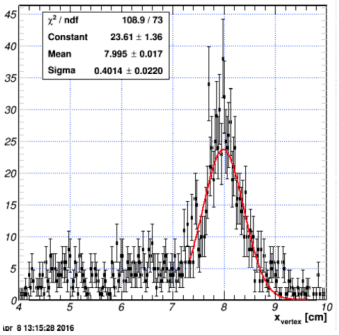

Figure 88

A new motherboard, FASP-Read-Out (FASPRO), was developed to house the FASP-02 chip, 16 ADCs, and the drivers for external connections. The board is driven by a 40 MHz clock, which can also be fed externally. Each differential output channel delivers digitized values of the signal amplitude and the corresponding channel-wise self-triggered time signal (Chip Select, CS). The output is prepared for GBTx integration, the solution foreseen for the CBM experiment to transmit data from the detector to the online/offline processing units (Fig.89).

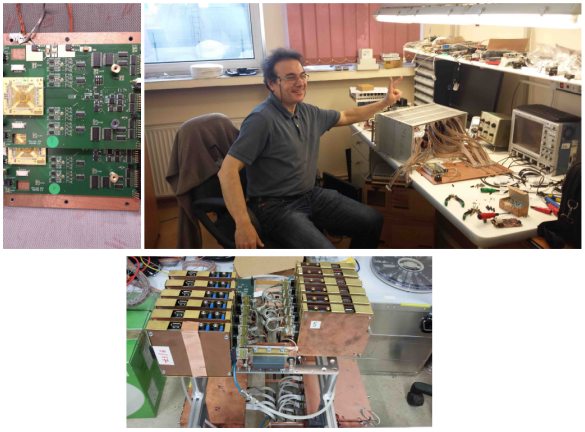

Figure 89

The free-running DAQ based on FASPRO boards was successfully tested during the CERN-SPS campaign with ^{208}Pb beams, using charged particles produced by 150 GeV/c ^{208}Pb on ^{208}Pb targets [C. Schiaua, private communication; A. Bercuci et al, CBM Progress Report 2016, pg.114].

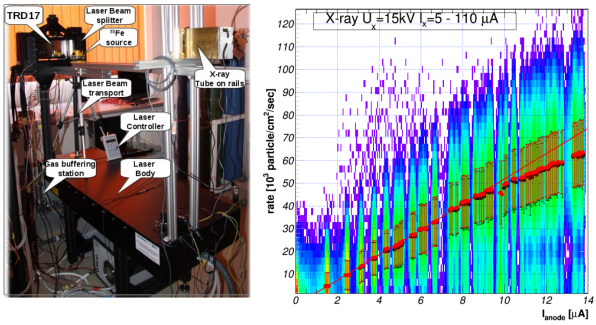

Figure 90

In-house high counting rate tests were performed using an identical TRD prototype with triangular pads. Two quartz windows were inserted along the wire direction on both sides, allowing three laser beams to be injected into the middle of each of the three row pads (Fig.90-left). A systematic scan of incident rates was conducted by changing the current on the X-ray tube (see Fig.90-right). The X-ray spectrum determined for U_x = 15 kV contained the α-, β-, and γ-lines of the Au target. Successive 2-minute irradiations were followed by 10-minute cooling periods. During the cooling periods, the ^{55}Fe source was measured while the laser spectrum was fired continuously at a rate of 10 Hz. The observed rate drop can be well explained by the conservative rate calculation used here and limitations in the data transfer [A. Bercuci et al., CBM Progress Report 2017, pg.89].

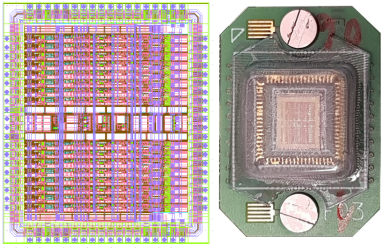

Figure 91

To further enhance the position resolution achievable with the new pad-plane architecture, a third version of FASP (v03) was designed and built for use in mCBM. This new version retains the features of the previous version but includes improved

analog circuitry and a DCS-selectable feature that processes channels not self-triggering but neighboring a channel with signals above a selected threshold. The designed, produced, and bonded FASP-v03 is presented in Fig.91 [V. Catanescu, private communication].
In parallel, a new version of FASPRO was designed and produced. The new FASPRO which includes 6 FASP chips and ADCs, the GETS (General Event Time-stamping Streamer) board with two FPGAs, and their integration scheme in the CBM data flow concept is shown in Fig.92 [C. Schiaua, private communication; A. Bercuci et al, CBM Progress Report 2018, pg79].

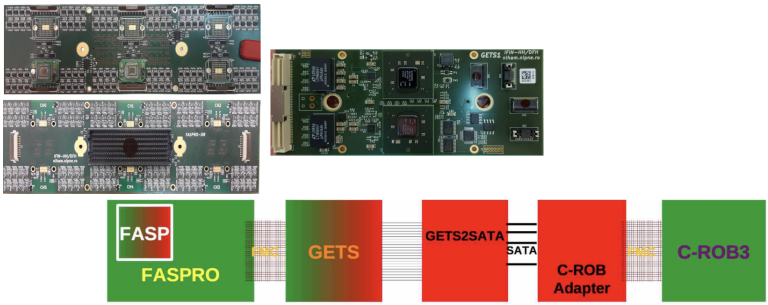

Figure 92

The advantages and performances of the TRD-2D architecture were decisive arguments for the CBM Collaboration to choose this solution for the inner zone of the TRD subdetector in the CBM experiment. An addendum for the Transition Radiation Detector 2D (TRD-2D) was approved (Fig.93) [A. Bercuci et al.].

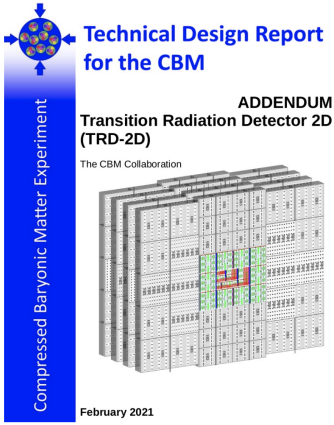

Figure 93

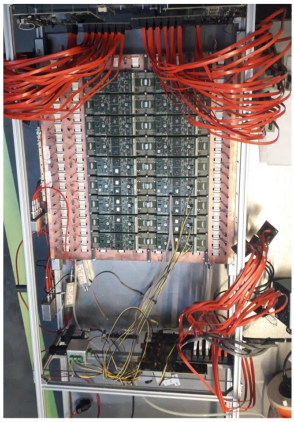

Figure 94

For in-beam tests at mCBM, a full-size prototype (60×60 cm^2) equipped with the new FEBs was transported to GSI (Fig.94). In-beam tests at SIS18 using Au+Au collisions at 1.13 A·GeV and mCBM configuration showed a position resolution of approximately 100 μm across the pads, excellent Particle Identification (PID) based on correlating TRD-2D dE/dx information with ToF velocity, and good tracking resolution (Fig.95) [A. Bercuci et al., 42nd CBM Collaboration Meeting, September, 25, 2023].

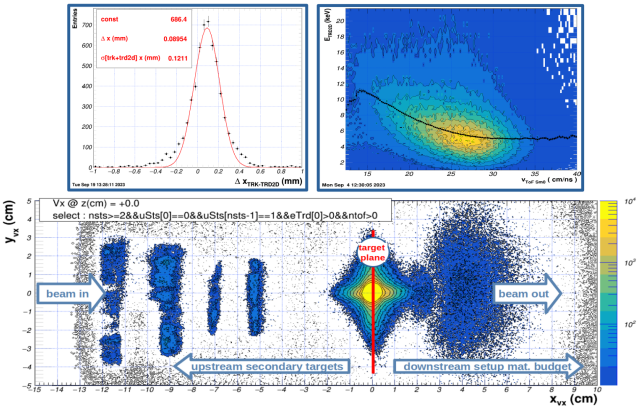

Figure 95

Systematic studies for different structures of the chamber's entrance window were performed, and the best structure was determined to be a combination of 100 μm carbon fiber foil, 25 μm aluminized Mylar, 9 mm honeycomb, and 20 μm aluminized Kapton foil [D. Dorobantu et al., CBM Progress Report 2021, pg.119].

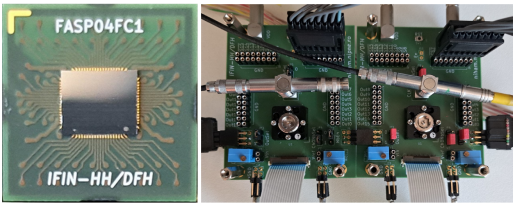

Figure 96

A new FEE board (FASPRO3-F) was designed and produced with 12 FASPs (new package) (Fig.96 - left BGA packaging, Fig.96 right new test board), 6 ADC chips (32 channels each), 3 PolarFire FPGAs, and side connectors for various configurations (Fig.97-left) [C. Schiaua, 42nd CBM Collaboration Meeting, September, 25, 2023; V. Catanescu and C. Schiaua, EUROPRACTICE Activity Report, 2023 - 2024)].

Currently, the full-size TRD-2D prototype is completely equipped with this new electronics (Fig.97 - right), and tests with pulser, ^{55}Fe radioactive source, and in-beam tests at mCBM are ongoing.
We are confident that the FAIR Council will make the right decision to include the CBM experiment in the "First Physics" stage of FAIR. Once approved, the in-kind contract to realize the entire inner zone of the CBM-TRD subdetector will be sent for signatures to access financial support from Romania for FAIR experiments.

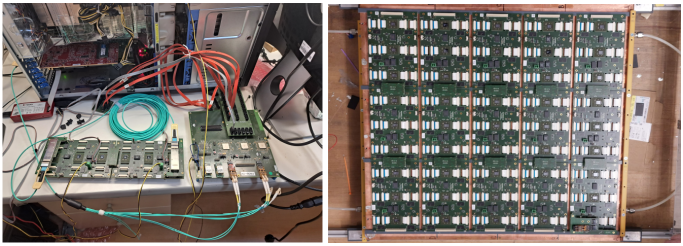

Figure 97

A simulation of image reconstruction of different shapes of the positron-emitting source using a barrel equipped with MSMGRPC is presented in Fig.98 [I. Berceanu et al, private communication].

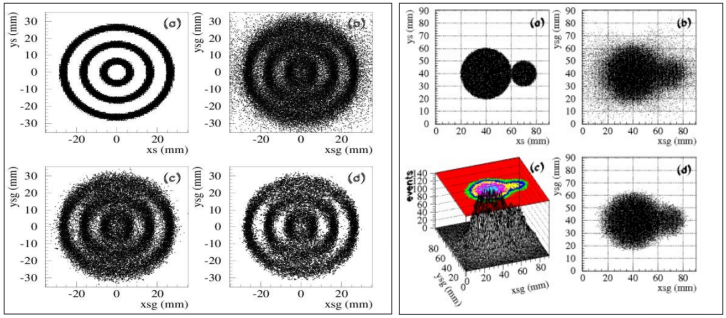

Figure 98

The capability of 2-D position measurements using TRD-2D was demonstrated by registering the image given by a ^{55}Fe X-ray source through a collimator (the letters "H", "P", and "D" of 2 mm thickness) cut out from a 45x27 mm^2 copper foil fixed on the entrance window of the detector (Fig.99) [A. Bercuci et al., private communication]. These results indicate that such detectors could be used for various applications.

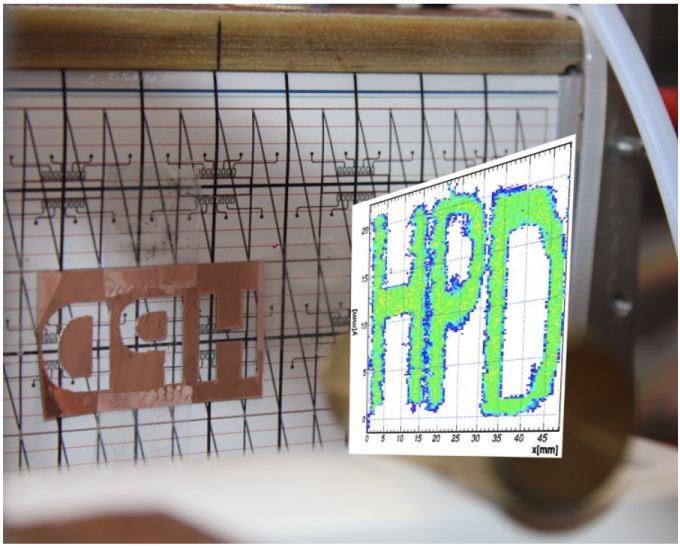

Figure 99

An overview of the main experiments carried out in-house using radioactive sources or in-beam tests at different accelerators over the past 20 years can be followed in the following photos.

2004
SIS18-GSI

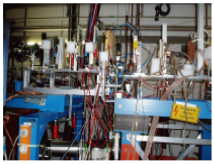

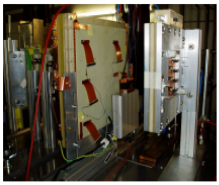

2005
SIS18 - GSI

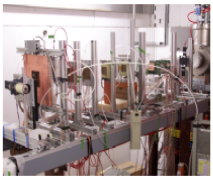

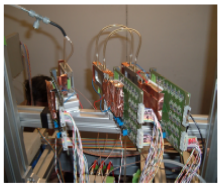

HPD - Bucharest

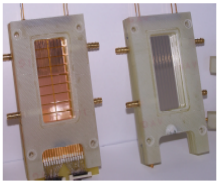

HPD - Bucharest

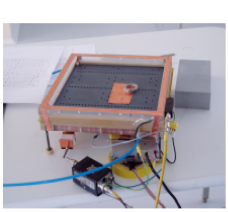

2008
ELBE Rosendorf

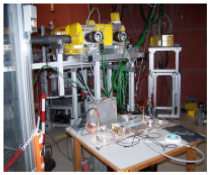

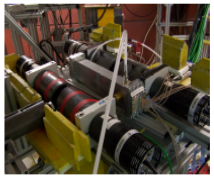

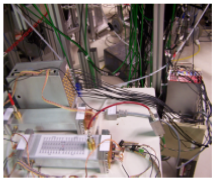

HPD - Bucharest

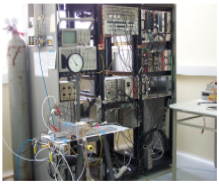

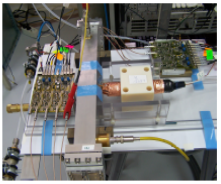

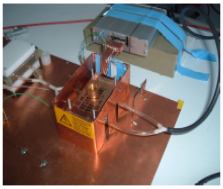

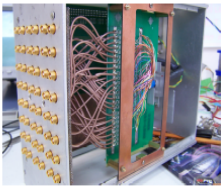

2009
SIS18-GSI

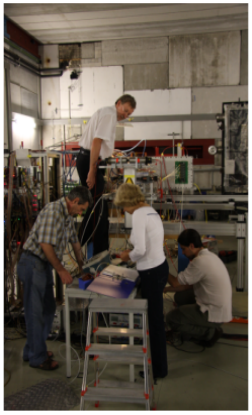

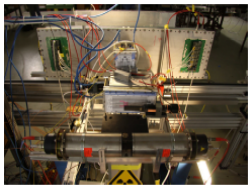

HPD - Bucharest

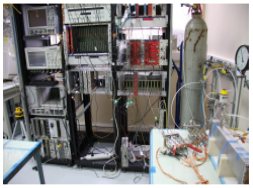

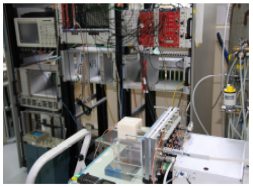

2010
PS-CERN
T10

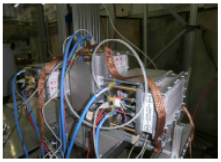

T9

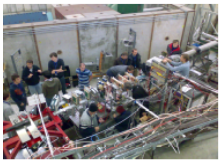

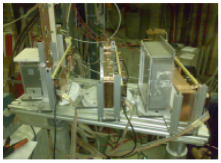

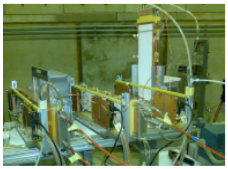

HPD - Bucharest

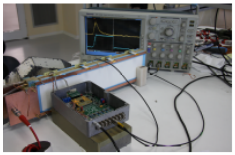

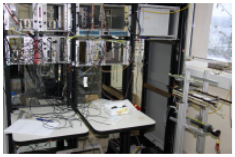

2011
PS-CERN
T10

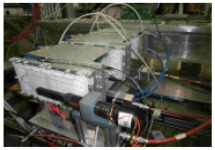

T9

COSY-Julich

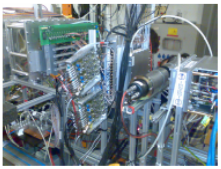

HPD - Bucharest

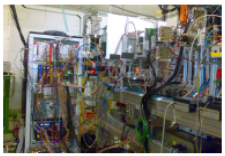

2012
SIS18 - GSI

T9
PS-CERN

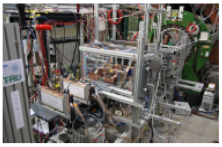

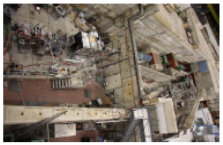

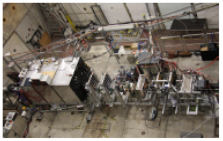

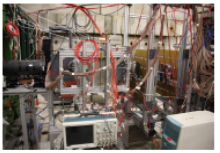

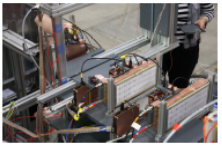

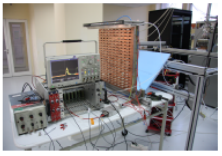

2014
SIS18 - GSI

PS-CERN
T9

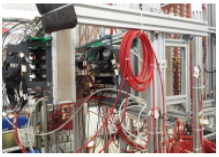

HPD - Bucharest

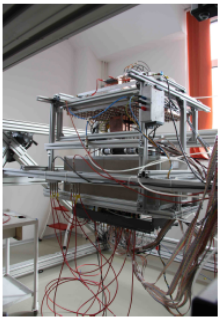

HPD - Bucharest

2015

SPS-CERN
H4

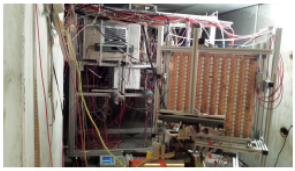
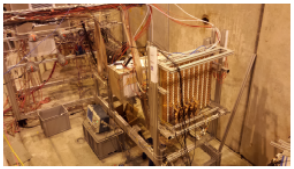
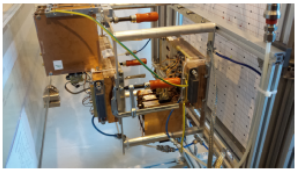
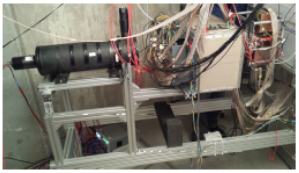
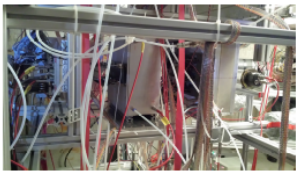

2016-2017

Integration in mCBM

@ SIS18

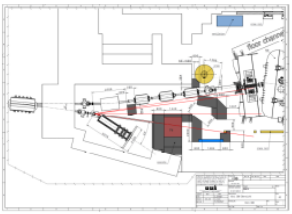
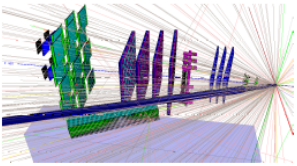

SPS-CERN
H4

HPD - Bucharest


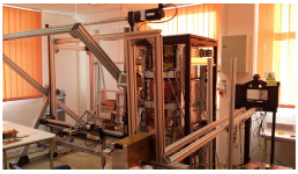

2018

mCBM @ SIS18

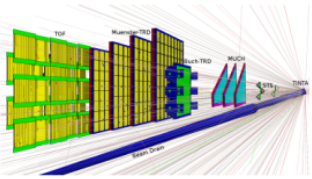

HPD - Bucharest


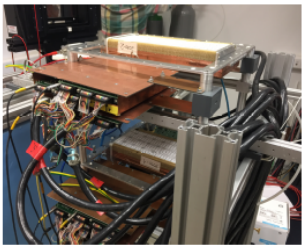

2019

mCBM @ SIS18

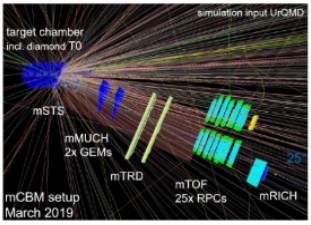

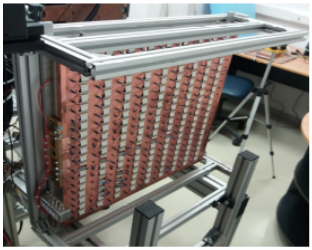

HPD - Bucharest

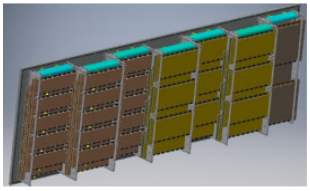

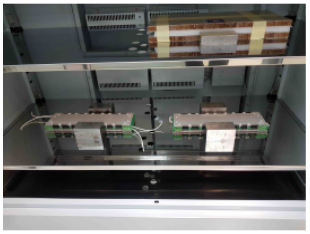

2020-2021

HPD - Bucharest

mCBM @ SIS18

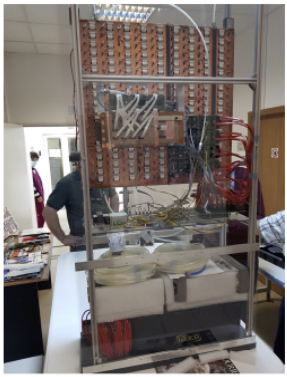

MPIR IFIN-HH Bucharest

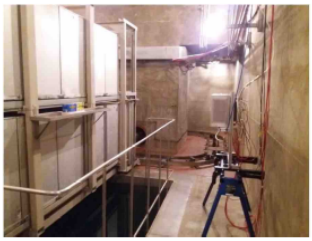

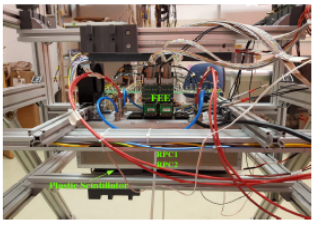

HPD - Bucharest

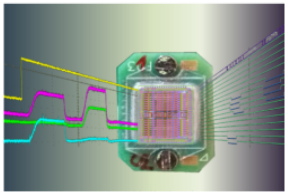

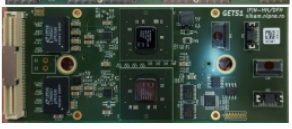

2022

mCBM @ SIS18

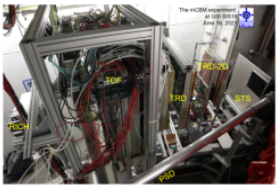

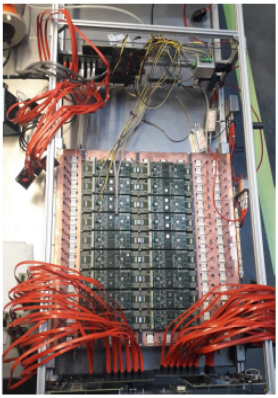

HPD - Bucharest

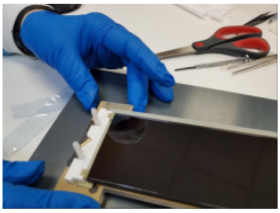

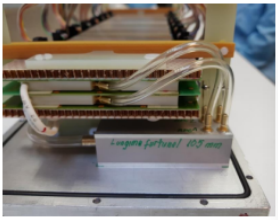

2023

mCBM @ SIS18

HPD - Bucharest

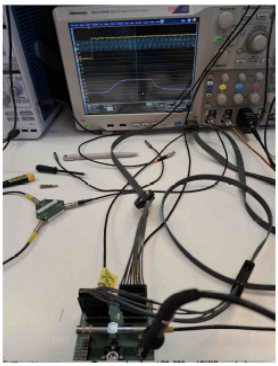

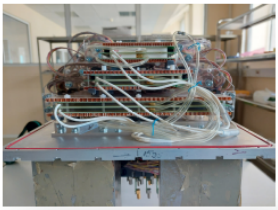

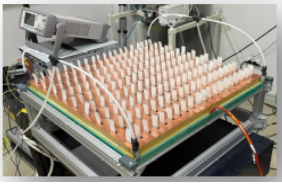

2024

mCBM @ SIS18

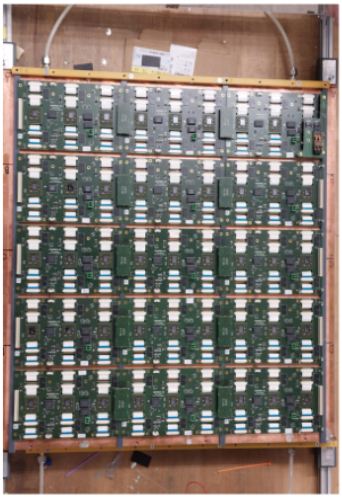

HPD - Bucharest

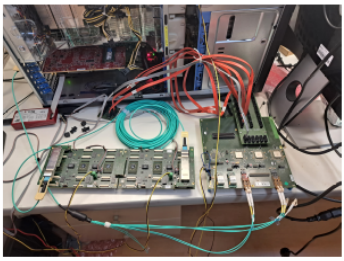

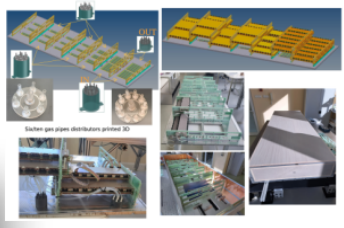

Obviously, the efforts invested in these activities were motivated by the physics which can be accessed using a unique experimental device like CBM in the energy regime of SIS100 at FAIR-Darmstadt. An overview of the main theoretical approaches towards understanding the properties of hot and dense matter in heavy-ion collisions, along with a compilation of relevant observables obtained at existing facilities, was presented and discussed about 20 years ago, in 2006, during workshops at ECT in Trento. Based on these discussions, a CBM Physics Book was edited [The CBM Physics Book (Compressed Baryonic Matter in Laboratory Experiments, Springer, Lecture Notes in Physics 814(2011))].

In the meantime, new theoretical and experimental results have been obtained, enlarging the discovery potential of the CBM experiment at SIS100. Below, we briefly mention some of these results and list a few types of studies requiring the measurement of p_T spectra down to very low values using the performance of the detectors described above, which could support or challenge theoretical expectations.

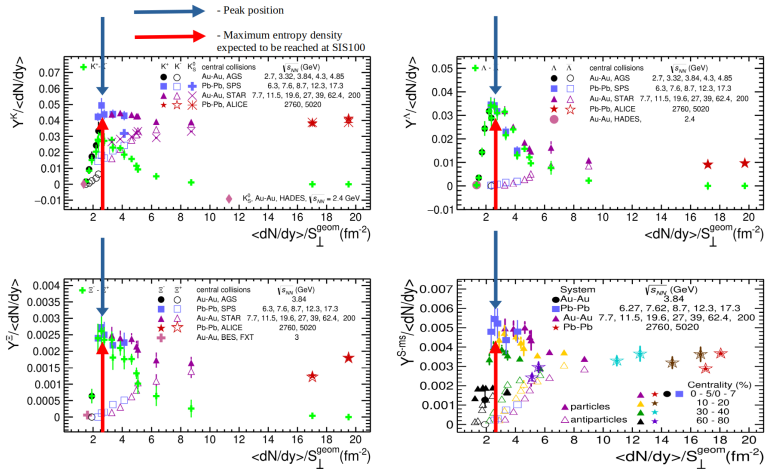

Figure 100

Based on the existing experimental results from AGS, SPS, BNL, RHIC, and LHC, we performed a systematic study of the correlation between the ratio of single- and multi-strange hadron yields per unit rapidity to the total particle multiplicity per unit rapidity and the entropy density as a function of the fireball size [A. Pop and M. Petrovici, arXiv:2402.19115[hep-ph]].

A maximum was evidenced in the $Y^S/\langle dN/dy\rangle - \langle dN/dy\rangle/S_\perp$ correlation for combined and separate species of strange hadrons at different centralities (Fig.100 - blue arrows; red arrows mark the value of expected entropy density per unit of transverse overlap area at the maximum SIS100 energy - $\sqrt{s_{NN}} = 4.9$ GeV), in the region where a transition from baryon-dominated matter to meson-dominated matter occurs (Fig.101).

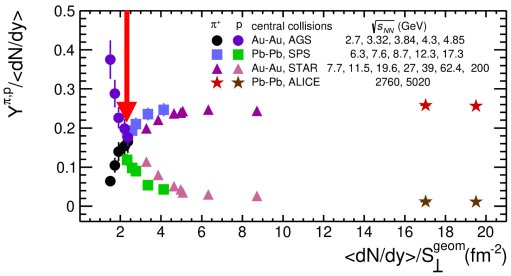

Figure 101

Within the PHSD transport approach [W. Cassing et al., Phys. Rev. C 93, 014902 (2016)], the strangeness enhancement up to the maximum is attributed to chiral symmetry restoration at high baryon density. Therefore, the position of the maximum could be indicative of a maximum baryon density of the fireball [J. Cleymans et al., Eur. Phys. J. A C93(2016)014902; W. Busza and A. Goldhaber, Phys. Lett. B 139(1984)235]. This value could be reached in central Au-Au collisions at the maximum SIS100 energy.

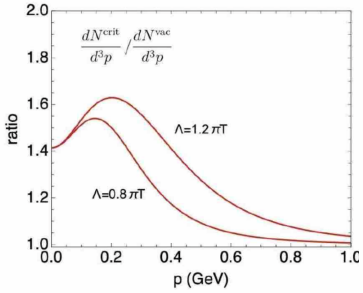

Figure 102

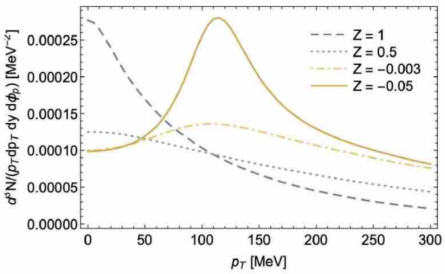

Figure 103

In a recent paper, the impact of fluctuations of the order parameter (σ, $\overrightarrow{\pi}$), expected to be enhanced near the QCD critical point, on the transport coefficients of QCD has been studied, predicting an enhancement of the soft pion yield (Fig.102) [E. Grossi et al., Phys. Rev. D 104 (2021) 034025]. To observe this experimentally, p_T values well below 200 MeV/c must be accessed. A maximum in the invariant transverse momentum spectra, as a signature of the moat regime in heavy ion collisions, was recently proposed [R.D. Pisarski and F. Rennecke, Phys. Rev. Lett.

127 (2021) 152302]. As seen in Fig.103, experimental information at p_T well below 100 MeV/c is essential. Such very low range in p_T can be reached by CBM based on the performance of the detectors presented above.

At SIS100 energies, one could reach baryon densities in Au-Au collisions in the region of $3.5\rho_0$, specific to the core of massive neutron stars. The requirement that neutron stars reach a maximum mass of at least $M_{\max} \geq 2M_\odot$ and have very small radii (Fig.104 - right) leads to equations of state (EoS) that predict a speed of sound c_s^2 surpassing the conformal limit of 1/3 and a large peak in c_s^2 as a function of baryon density n_B and pressure-energy density correlation (Fig.104 - left), indicating the rough location of the deconfinement transition [E. Annala et al., Nature Physics 16 (2020) 907].

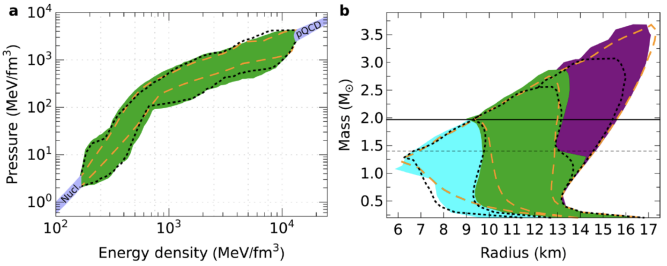

Figure 104

The natural question is to what extent such a requirement is compatible with the EoS extracted from heavy ion data, given the significant differences between a $M = 2M_\odot$ neutron star and a fireball produced in heavy-ion collisions, i.e., 18 orders of magnitude in size, over 35 orders in lifetime, the neutron star temperature being close to zero while the baryonic fireball has a temperature in the region of 40-120 MeV and is nearly symmetric ($\delta = (n_n - n_p)/(n_n + n_p) \approx 0$). One should also consider the fireball's violent dynamical evolution, its highly non-homogeneous initial state, finite size effects, and the in-medium and isospin momentum dependence of nucleon-nucleon interactions.

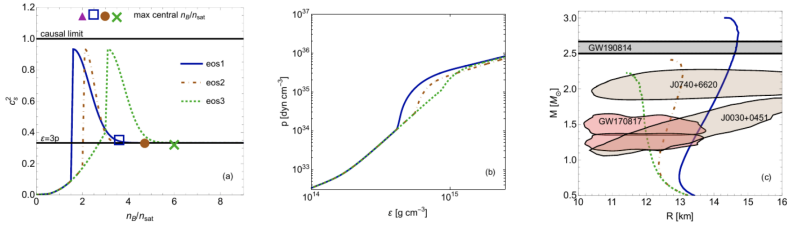

Figure 105

In a recent work, using the symmetry energy expansion, equations of state for massive neutron stars predicting a steep rise in the speed of sound (Fig.105) have been obtained and implemented in a hadronic transport code, SMASH [N. Yao et al., arXiv:2311.18819 [nucl-th]]. The features of the EoS explaining the mass and size of neutron stars were also reproduced using a quarkyonic description, where a rapid change in the sound velocity is related to the transition to the quarkyonic regime, and a similar structure is observed in the trace anomaly - $\triangle$ (Fig.106) [L. McLerran, Symmetry 15 (2023) 1150].

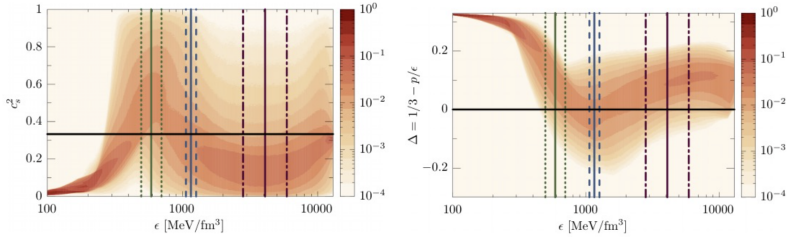

Figure 106

Within the same approach, a nuclear matter regime is expected at low density while the high-density regime corresponds to the quarkyonic regime. In the quarkyonic regime, baryons are depleted at low momenta and produce a momentum shell (Fig.107) [Y. Fujimoto et al., Phys. Rev. Lett. 132 (2024) 112701].

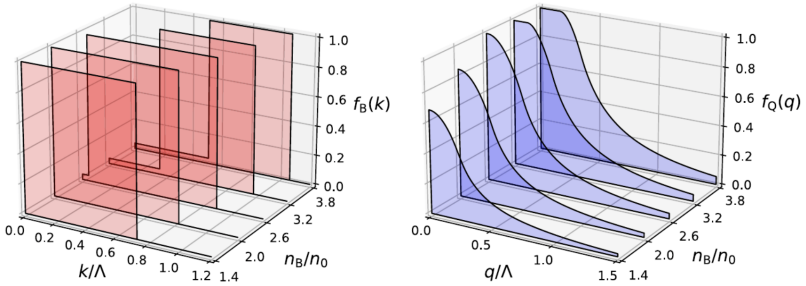

Figure 107

To support or refute such very appealing theoretical predictions, multi-differential analysis for different hadrons, especially the strange and multi-strange ones, is

mandatory. Among others, we would mention the following, dedicated analysis:

Excitation function for collision geometry and azimuthal dependence of:

- p_T spectra as low as possible in p_T

  $-\pi,\ k,\ p$
  $-\Lambda,\ \Xi,\ \Omega$

- slope and offset of $\langle p_T \rangle$ as a function of mass

  $-\pi,\ k,\ p$
  $-\Lambda,\ \Xi,\ \Omega$

- $\langle \beta_T \rangle$ and $T_{\rm kin}$ BGBW fit parameters

  $-\pi,\ k,\ p$
  $-\Lambda,\ \Xi,\ \Omega$

- Core-Corona $\Rightarrow$ pp collisions at the same energies, mandatory
- IMFs (^{3}He vs. ^{3}H)
- Different A-A and N/Z symmetric colliding systems

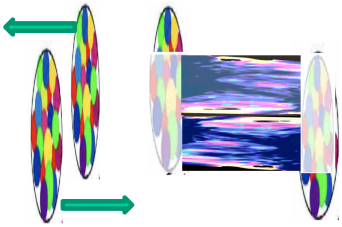

Figure 108

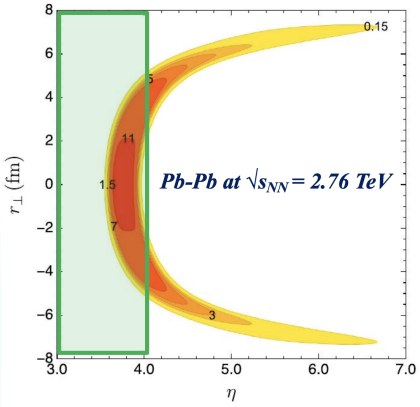

Figure 109

Worth mentioning is the fact that this new generation of MSMGRPC and TRD-2D could be considered as a solution for large rapidity coverage at LHC in terms of PID, where, based on CGC approach, the residing nuclei from A-A collision (Fig.108-left) are supposed to have baryon density more than ten times of normal nuclear matter density (Fig.108-right)[M. Li and J.I. Kapusta, Phys. Rev. C 99 (2019) 014906].

The main, present and former, actors behind the achievements summarized above:

Cristian Andrei, Oana Andrei, Valerica Aprodu, Daniel Bartos, Ionela Berceanu^{+}, Alexandru Bercuci, Gheorghe Caragheorgheopol, Vasile Catanescu, F. Constantin* Gheorghe Dima, Petre Dima^{+}, Constanta Dinca, Dan Duhovnicu*, Marin Duma*, Viorel Duta, Gheorghe Giolu*, Andrei Herghelegiu, Elena Ionescu*, Constantin Magureanu*, Gheorghe Mateescu, Dorin Moisa*, Mariana Petris, Alexandrina Petrovici, Mihai Petrovici, Amalia Pop, Lucia Prodan*, Andrei Radu, Laura Radulescu, Claudiu Schiaua, Victor Simion^{+}, George Stoian, Madalina Tarzila, Petre Zaharia*.
(* former members, + deceased)

The results summarized here were made possible thanks to substantial financial support for setting up the appropriate local infrastructure, funding for manpower, travel, and working periods in different research centers where in-beam tests were conducted. This support was provided by the Coordinating Ministry, the Institute of Atomic Physics, Hadron Physics EU projects, and various projects within national programs such as those mentioned here:

We extend our gratitude to the following institutions for their outstanding support in all respects, including general infrastructure, excellent operating crews, and the overall atmosphere during the in-beam tests.

Additionally, we express our special thanks to the colleagues from the CBM Collaboration who, in various ways, contributed to the successful in-beam test campaigns.

This issue of HPD Courier is dedicated to the 20th anniversary of the CBM Collaboration.

Ministerul Cercetării,
Inovării şi Digitalizării

20th Anniversary of CBM Collaboration

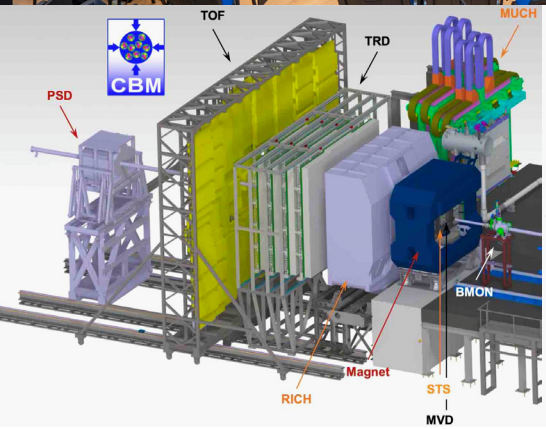

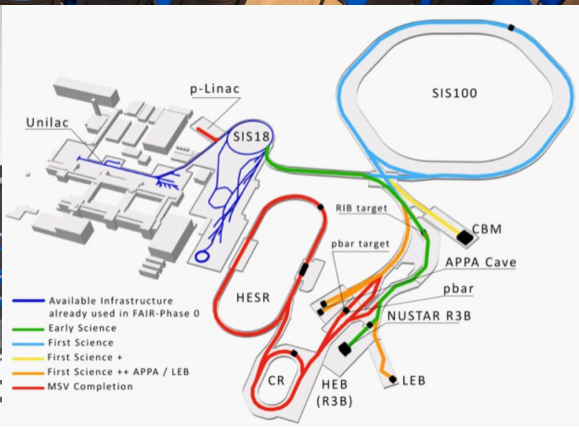

Contact
Prof. Dr. Mihai Petrovici
Email: mpetro@nipne.ro

Editors
Mădîlina Târzilă and Mihai Petrovici
Production editor: Adrian Socolov